INTERACTION OF PULMONARY SURFACTANT PROTEIN A (SP-A) WITH DPPC/egg-PG BILAYERS

NIDAL M. ABU-LIBDEH

Your file Votre référence
ISBN: 0-612-89607-2
Our file Notre référence
ISBN: 0-612-89607-2

Interaction of Pulmonary Surfactant Protein A (SP-A) with DPPC/egg-PG Bilayers

by

© Nidal M. Abu-Libdeh
M.Sc. (2000) Yarmouk University, B.Sc. (1997) Yarmouk University

A thesis submitted to the
School of Graduate Studies
in partial fulfillment of the
requirements for the degree of
Master of Science.

Department of Physics and Physical Oceanography
Memorial University of Newfoundland

January 8, 2003

ST. JOHN'S NEWFOUNDLAND

Contents

Abstract iv

Acknowledgements vi

List of Figures x

Abbreviations xi

1 Introduction 1

1.1 Pulmonary Surfactant System 1

1.1.1 Composition of Surfactant 2

1.1.2 Role of Surfactant Proteins 5

1.2 Previous ^{2}H-NMR Studies of Phospholipids/ Surfactant-Protein Interaction 8

1.3 Objective of this Work 12

2 ^{2}H-NMR Theory 14

2.1 The Electric Quadrupole Interaction 15

2.2 ^{2}H Quadrupolar Hamiltonian in the presence of Molecular Motion . . 20

2.3 The Quadrupole Echo 23

2.3.1 Quadrupole Echo Formation 24

2.3.2 Molecular Motions and ^{2}H Quadrupolar Relaxation 27

3 Experimental Setup and Details **31**

3.1 ^{2}H-NMR Experimental Setup 31

3.2 Experimental Details 33

3.3 Sample Preparation 34

4 Results and Discussion I: SP-A Effect on DPPC Acyl Chain **37**

4.1 Introduction 37

4.2 Electron Microscopy Results 38

4.3 ^{2}H-NMR Results 39

4.3.1 ^{2}H-NMR Spectra and First Spectral Moment 40

4.3.2 Deuteron Transverse Relaxation 46

5 Results and Discussion II: SP-A Effect on DPPC Headgroup **51**

5.1 Introduction 51

5.2 Interaction of SP-A with DPPC Headgroup 53

6 Summary and Concluding Remarks **57**

Abstract

Surfactant protein A (SP-A) is the major protein component of pulmonary surfactant, a material that reduces surface tension at the air-water interface in lungs. This reduction is achieved by forming a phospholipid monolayer. Formation of the monolayer is thought to proceed via an intermediate structure, tubular myelin, in which lipid bilayers are arranged in a lattice of tubes. The minimum requirement for formation of tubular myelin *in vitro* appears to be the saturated lipid dipalmitoylphosphatidylcholine (DPPC), anionic lipid egg-phosphatidylglycerol (PG), the hydrophobic protein SP-B, and the hydrophilic protein SP-A. SP-A is an octadecamer which is thought to interact with the bilayer surface through its carbohydrates recognition domain (CRD). The interaction of SP-A with DPPC/egg-PG bilayers, in the presence of calcium and with or without SP-B, has been studied using deuterium NMR observations of chain and headgroup deuterated DPPC in protein-lipid mixtures. While the DPPC-d_{62}/egg-PG bilayers liquid crystal-to-gel phase transition was found to proceed continuously in the presence of only SP-A, it was relatively sharp in the presence of SP-A and SP-B. SP-A alone reduces the first spectral moment M_1 for DPPC-d_{62}/egg-PG bilayers in the gel phase. When it is incorporated with SP-B into the DPPC-d_{62}/egg-PG bilayers the first spectral moment, M_1, was found, in the gel phase, to be higher than for the protein-free lipid mixture. These observations suggest that SP-A alone does not remove the effect of egg-PG on the DPPC bilayers

and, hence, it has no specific interaction with either lipid component of the mixture. The removal of the effect of egg-PG on DPPC bilayers by SP-A and SP-B together suggests that SP-B may have a preferential interaction with egg-PG or that both proteins interact in a cooperative manner with the egg-PG. Transverse relaxation time (T_{2e}) studies suggest that SP-A influences slow lipid motions in the liquid crystalline phase. DPPC headgroup studies showed that the presence of SP-A reduces the size of the β quadrupole splittings while the α quadrupole splittings remains unchanged. This was found to be consistent with the increase in area per lipid and, at the same time, with a decrease in the headgroup orientational order resulting from interaction with SP-A. Taken together, these observations are consistent with the expectation that SP-A interacts primarily at the bilayer surface.

Acknowledgements

I wish to express my deep gratitude to my supervisor Professor Michael Morrow for providing the facilities and for giving me the opportunity to work and learn new things in his research group. His expertise, combined with kind patience and unbelievably positive attitude have helped and encouraged me many times during the years of my study.

This work wouldn't have been possible without the collabration of Dr. K. M. W. Keough and his group from the Department of Biochemistry. I would like to express my special thanks to June Stewart for preparing all samples studied in this work and for providing the electron micrographs.

I am grateful to School of Graduate Studies and Department of Physics and Physical Oceanography for financial support as a form of fellowship and graduate assistantship.

It is my pleasure to acknowledge the help of departmental workshop and the university technical services; especially, I would like to thank Wayne Holly for keeping our lab. going with an excellent cryogenic facility. Without the excellent facilities and friendly staff of the physics Department, my work would have been extremely.

It is a great pleasure to thank all the members of our research group: David Goodyear, Ian Skanes and André Brown for their valuable discussion and unlimited help they gave it to me. With them I spent a great time.

Finally, I wish to give my warm thanks to my nearest and dearest, including my family in Jordan, my wife Niveen for their understanding, encouragement and support. Warm thanks to my son Alaa for the most precious things in life.

St.John's, NL, Canada, December 2002

Nidal Abu-Libdeh

List of Figures

1.1 Schematic space-filling representation of dipalmitoylphosphotidylcholine (DPPC). DPPC is zwitterionic with a temporary dipole. 3

1.2 Schematic structure of SP-A. Six SP-A trimers associated to form a flower bouquet-like structure. 4

2.1 Splitting of the Zeeman energy levels by the quadrupole interaction. . 17

2.2 (a) C-^{2}H bond orientation and (b) splitting for single deuteron. . . . 19

2.3 Model powder spectrum for phospholipids deuterated in a single acyl chain position. The sharp shoulders and peaks of the spectrum are broadened in real systems. The vertical axis is intensity. 21

2.4 Quadrupole echo pulse sequence and the echo formation. 24

2.5 Quadrupolar echoes as a function of pulse spacing (τ). 29

3.1 Block diagram of 9.4 T NMR spectrometer. 32

4.1 Electron micrographs of (A) 51% DPPC-d_{62}, 22% egg-PG, 16% SP-A and 11% SP-B, (B) 66% DPPC-d_{62}, 24% SP-A and 10% SP-B, (C) DPPC-d_{62}/egg-PG (7:3) and (D) DPPC-d_{62}/egg-PG (7:3) with 16% SP-B. All samples were hydrated in buffer containing 5 mM Ca^{2+}. Bars represent 500 nm. 39

4.2 Temperature dependence of the ^{2}H-NMR spectrum of DPPC-d_{62}/egg-PG (7:3) bilayer (*left*) and a bilayer with 16% (w/w) SP–A (*right*). Both samples were hydrated in buffer containing 5 mM Ca^{2+} 42

4.3 Temperature dependence of the ^{2}H-NMR spectrum of DPPC-d_{62}/egg-PG (7:3) bilayer with 16% (w/w) SP–A and 11% (w/w) SP–B hydrated in buffer containing 5 mM Ca^{2+}. 43

4.4 Temperature dependence of ^{2}H-NMR first spectral moments for DPPC-d_{62}/egg-PG (7:3) bilayer with (open circle) no protien, (diamond) 16% SP-A and 11% SP-B, and (solid circle) 16% SP-A. 44

4.5 DePaked ^{2}H-NMR spectra for DPPC-d_{62}/egg-PG (a) without SP-A and (b) with SP-A. 45

4.6 Quadrupole echo deacy for DPPC-d_{62}/egg-PG bilayer (*left*) and the sample containing 16% (w/w) SP-A (*right*). 47

4.7 Temperature dependence of T_{2e} for DPPC-d_{62}/egg-PG bilayer (open) and the sample containing 16% (w/w) SP-A both hydrated in buffer containing 5 mM Ca^{2+}. 48

4.8 Temperature dependence of T_{2e}: Slow and fast motions contribute differently to the relaxation. 49

5.1 The phosphatidylcholine headgroup showing the α and β deuterons. **D** denotes a deuteron. 52

5.2 Temperature dependence of the ^{2}H-NMR spectrum of DPPC-d_4/egg-PG (7:3) bilayer (*left*) and a bilayer having 16% (w/w) SP–A (*right*) both hydrated in buffer containing 5 mM Ca^{2+} 54

5.3 Temperature dependence of headgroup deuteron quadrupole splittings for the sample with SP-A (*solid symbols*) and without SP-A (*open symbols*) for the α (*squares*) and β (*circles*) headgroup deuterons. . . 55

Abbreviations

RDS:	Respiratory Distress Syndrome
^{2}H-NMR:	Deuterium Nuclear Magnetic Resonance
PC:	Phosphatidylcoline
DPPC:	1,2-dipalmitoyl-sn-glycero-3-phosphocholine
PG:	Phosphatidylglycerol
DPPG:	1,2-dipalmitoyl-sn-glycero-3-phosphoglycerol
egg-PG:	phosphatidylglycerol mad from egg yolk phosphatidylcholine
PI:	Phosphatidylinositol
PE:	Phosphatidylethanolamine
PS:	Phosphatidylserine
SP-A:	Surfactant Protein A
SP-B:	Surfactant Protein B
SP-C:	Surfactant Protein C
SP-D:	Surfactant Protein D
CRD:	Carbohydrate Recognition Domain
DPPC-d_{62}:	1,2- perdeuterodipalmitoyl-sn-glycero-3-phosphocholine
DPPG-d_{62}:	1,2- perdeuterodipalmitoyl-sn-glycero-3-phosphoglycerol
DPPC-d_4:	1,2- dipalmitoyl-sn-glycero-3-phospho-(α, β perdeutero)-choline

Chapter 1

Introduction

1.1 Pulmonary Surfactant System

Pulmonary surfactant is a complex mixture of surface active phospholipids and specific proteins, synthesized and secreted by alveolar type II cells [1]. Pulmonary surfactant reduces the surface tension of the air-water interface at the alveolar surface and hence prevents alveolar collapse. This reduction is achieved by forming a stable monolayer or film of surfactant phospholipids [1–3]. A lack of surfactant causes a disturbance in alveolar gas exchange. This can be seen in premature infants suffering from respiratory distress syndrome (RDS), a major cause of neonatal death [1]. Pulmonary surfactant, packed into lamellar bodies, goes through several transformations before it adsorbs at the air-water interface as a monolayer. In order to get a clear understanding of the system and questions addressed in this work, a brief review of the composition of the surfactant system and the physiological roles of surfactant proteins are presented here. The remainder of this chapter concentrates on previous deuterium nuclear magnetic resonance (^{2}H-NMR) studies of the phospholipid/surfactant-protein system that serve to introduce the present work.

1.1.1 Composition of Surfactant

Pulmonary surfactant is composed of two main components: lipids and surfactant-specific proteins [1, 4]. Lipids account for approximately 90% of surfactant mass. Of surfactant lipids, 80 - 90% are phospholipids. Other lipids that are found include cholesterol, triacylglycerol, and free fatty acids. Phosphatidylcholine (PC) is identified as the most abundant component of surfactant and is always found in a quantity of 70-80% of the total amount of phospholipids. Approximately 60-70% of PC is saturated, especially in the dipalmitoylate form (DPPC), which accounts for about 50% of total surfactant lipids. DPPC is the major surface-active component. The disaturated nature of DPPC enables surfactant to withstand very high surface pressure, and this is thought to prevent the collapse of the alveoli and conducting air ways [1–3]. Figure 1.1 shows a schematic space-filling representation of DPPC. The acidic phospholipids, phosphatidylglycerol (PG) and phosphatidylinositol (PI) comprise approximately 8-15% of the total surfactant phospholipids in most species. The remaining phospholipids in surfactant are phosphatidylethanolmine (PE) and phosphatidylserine (PS), which are present in rather small amounts [4].

Although most of surfactant consists of lipids, it also contains approximately 10% proteins. Four surfactant-associated proteins have been identified and they can be divided into two groups: the hydrophilic surfactant proteins SP-A and SP-D, and hydrophobic proteins SP-B and SP-C [1, 4, 5, 7]. SP-D, with a mass of 43 kDa, is the largest surfactant protein. It is probably made up of at least four discrete structural domains [6, 7]. SP-D does not seem to have a role in the classical function of surfactant. Most putative functions described so far are related to lung host defense [7, 8].

SP-B is a 17.4 kDa hydrophobic protein of 79 amino acid residues, known for its

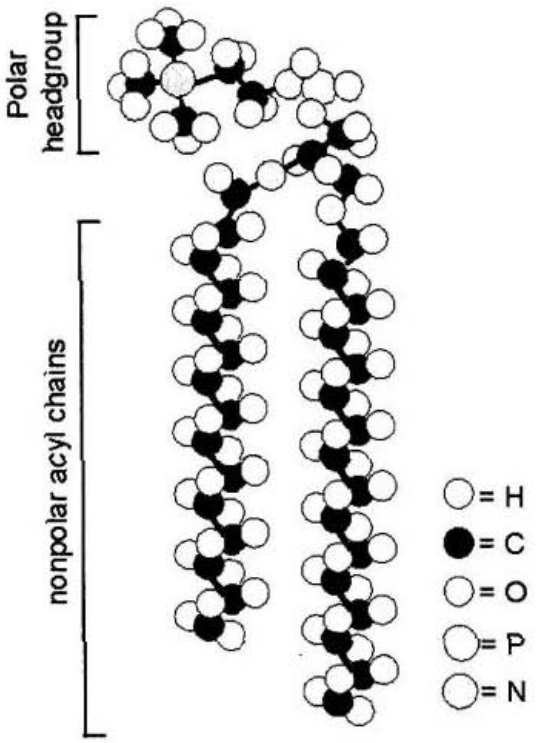

Figure 1.1: Schematic space-filling representation of dipalmitoylphosphotidylcholine (DPPC). DPPC is zwitterionic with a temporary dipole.

high cysteine content [8, 9]. The cysteine residues form a unique disulfide pattern of three intramolecular disulfide bonds and one intermolecular disulfide bond, which stabilize the protein and produce a dimeric form of SP-B [8, 9]. The secondary structure of SP-B is mainly α-helical [10]. The helices have an amphipathic character. SP-C is the smallest surfactant protein of 35 amino acid residues with apparent molecular weight of 4.2 kDa [9]. The protein is extremely hydrophobic, and is characterized by a high content of valine residues. Two thirds of the protein consist of a continuous hydrophobic stretch, and the secondary structure of this part of the protein is a regular α-helix [11], which is able to span a DPPC bilayer [12–14].

SP-A, which is the main subject of this work, was the first surfactant protein

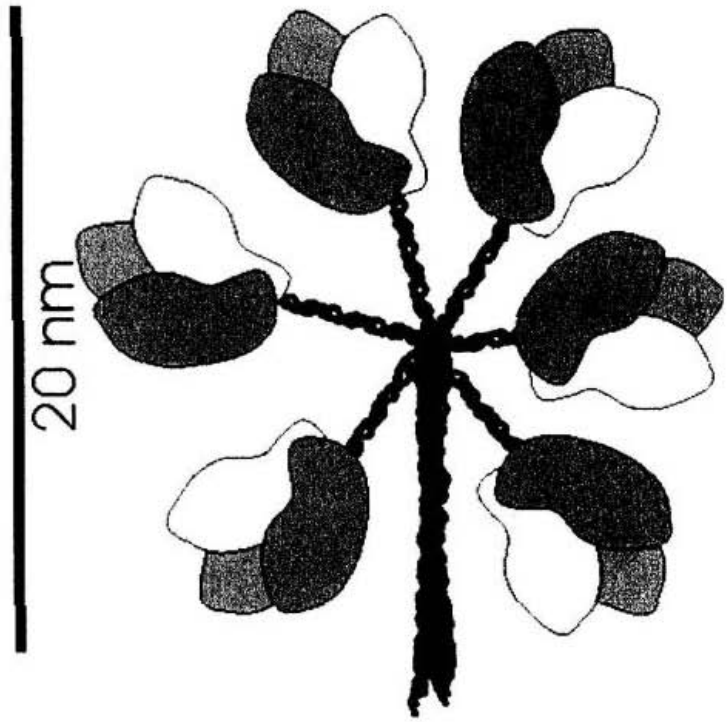

Figure 1.2: Schematic structure of SP-A. Six SP-A trimers associated to form a flower bouquet-like structure.

to be identified, and is also the major protein component of pulmonary surfactant [5, 6, 15, 16]. Human SP-A protein is encoded by two genes, SP-A1 and SP-A2, which are 94% identical in nucleotide sequence and 96% identical in amino acid sequence [17–19]. In the lung alveolus, human SP-A forms trimers that are thought to be composed of two SP-A1 molecules and one SP-A2 molecule [18–20]. As depicted in figure 1.2, the native SP-A protein is made up of six SP-A trimers that form a "flower bouquet"-like structure with monomeric molecular mass of 28-36 kDa [20]. The deduced primary structure of SP-A protein consists of four domains: an amino-terminal acid domain, a collagenous domain, a neck domain, and a C-terminal globular carbohydrate recognition domain (CRD). The amino-terminal of the SP-A molecule is a short peptide of 7 amino acids, with a cysteine residue at position 6 that aids in

the formation of interchain disulfide bonds between SP-A molecules. The collagenous domain of human SP-A is a 73-amino acid collagen-like segment, containing a series of 23 glycine-X-Y tripeptide repeats, with Y most often being a hydroxyproline and X being any amino acid [17]. Cysteine residues involved in SP-A trimer formation are also found in this region. An interruption occurs after the 13th glycine-X-Y tripeptide repeat in SP-A, with a proline residue inserted that introduces a flexible kink in the collagen region. This kink causes the trimers to bend outward in different directions, giving the mature SP-A octadecamer a flower bouquet appearance [20]. The neck region of SP-A consists of a short sequence of hydrophobic residues and an amphipathic helix, whereas the CRD contains a calcium-dependent carbohydrate binding site [21]. Several studies indicate that SP-A, in the presence of Ca^{2+}, interacts with phosphotidylcholine bilayers through its globular CRD [22, 23].

1.1.2 Role of Surfactant Proteins

Pulmonary surfactant is synthesized by alveolar type II cells. Surfactant material is stored within these cells in subcellular organelles called "lamellar bodies"[1, 4, 24, 25] These lamellar bodies contain almost all of the surfactant components and, hence, the release of the lamellar bodies may be regarded as equivalent to surfactant secretion [1, 24].

After the lamellar bodies are synthesized and secreted by alveolar type II cells, the material in the form of bilayers is believed to assume a geometric lattice-like structural morphology known as tubular myelin [1, 25, 26]. This structure contains elongated tubes which form a square lattice. Tubular myelin is thought to retain surfactant phospholipids in the alveolus until they spread into the monolayer that lines the alveolus. Pulmonary surfactant components (lipids and proteins) must interact

in a very specific way to generate these properties. It is known that the interaction of surfactant proteins with lipid mixtures in lung surfactant has an important role in forming the monolayer which decreases the surface tension of the material lining the alveoli [1–3, 25]. This monolayer is highly enriched in DPPC which enables surfactant to reduce the surface tension at the air-water interface of the alveoli. PG has been reported to have an actual physiological function in surfactant, which would be to facilitate the spreading and adsorption of the DPPC monolayer at the air-water interface [27]. The particular role of the other lipid components remain uncertain. The functions of the surfactant-associated proteins have been proposed based on many experimental results obtained by using a variety of techniques including transmission electron microscopy (TEM) [22, 26, 28], single particle electron crystallography [23], electron microscopy [29–31], epifluoresence microscopy [32], rhomboid surface balance [33, 34], and fluorescence studies [35–37]. Excellent reviews of all functions of the surfactant-associated proteins are available [1, 5, 38].

The hydrophobic proteins SP-B and SP-C have been reported to enhance the adsorption and surface tension-lowering properties of surfactant phospholipids required for normal lung function [39, 40]. SP-D is the most recently discovered pulmonary surfactant protein, and its functional properties in the surfactant system are not yet clear. As pointed out above, most proposed functions for SP-D are related to lung host defense.

The properties and putative functions of the hydrophilic protein SP-A have been studied more extensively than those of the other surfactant proteins [18, 22, 23, 26, 28–33, 38, 41–44]. SP-A in the presence of Ca^{2+}, is crucial in the conversion of pulmonary surfactant lamellar bodies into tubular myelin [26, 28, 29, 41]. It has also been detected in the corners of the square lattice in the cross-section of the tubular myelin and along the edges of its longitudinal axis [26, 41]. Tubular myelin is thought to be an

important intermediate lipid form that is essential for efficient interconversion of the secreted lamellar bodies to the surfactant film that lines the alveoli. Suzuki *et al.* [29] ran recombination experiments using synthetic lipids with extracted SP-A and SP-B proteins, and have shown that the minimum compositional requirement for the observation of tubular myelin *in vitro* was the presence of SP-A, SP-B, DPPC, PG, and calcium. The number of lattice structures formed were found to be dependent on the amount of both types of proteins. The presence of only one of the proteins was insufficient to form lattice structure. A study by Williams *et al.* [30] shows that a combination of SP-A and SP-B in DPPC/egg-PG bilayers results in reorganization of some the lipid into tubular myelin. SP-B and SP-C alone or in combination, as well as an SP-A/SP-C combination, had no effect on the structure of the lipid mixture. In this study, SP-A alone favored lipid aggregation but did not allow the tubular myelin to form. It is possible that, rather than simply promoting tubular myelin formation, SP-A is an essential component for its formation.

A second physiological function of SP-A is thought to be surfactant homeostasis. This putative function of SP-A has been suggested because the protein modulates the uptake and secretion of phospholipids by isolated alveolar type II cells *in vitro* [38]. Hawgood *et al.* [42] have shown that SP-A interacts with SP-B in a cooperative manner to further enhance phospholipid adsorption. Thin layer chromatography and fluorescence studies have shown that SP-A binds avidly to DPPC but less strongly to PG [35, 43]. SP-A binding to phospholipids has been shown to be calcium-independent. These properties may be important for enriching the surface monolayer with DPPC during hydrophobic surfactant protein-induced insertion of phospholipids into the monolayers.

Other putative functions of SP-A include enhancement of the biological activity of phospholipid extracts and binding of complex carbohydrates. Various studies suggest

that SP-A is involved in innate immune responses in the lung via its ability to bind various pathogens including viruses, bacteria, fungi, and particulates such as pollen grains and mite allergens [38]. For more details about SP-A's functions, the reader can refer to [1, 5, 38]

1.2 Previous ^{2}H-NMR Studies of Phospholipids/ Surfactant-Protein Interaction

The presence of a predominantly DPPC surfactant monolayer at the air-water interface within alveoli significantly reduces resistance to lung inflation as a result of surface tension. The function and composition of pulmonary surfactant and the structure of lung surfactant proteins have been reviewed in the previous sections. Surfactant material, in the form of lamellar bodies, is secreted into the aqueous layer by type-II pneumocytes in the alveolar wall. Maintenance of surfactant function requires the rapid spreading of material into the monolayer when lung volume is high and, presumably, refinement of the monolayer to its DPPC-enriched state as lung volume decreases [1–3, 25]. The transformation from lamellar body to monolayer, as mentioned previously in this chapter, appears to proceed via a loose arrangement of bilayers packed in an unusual form, tubular myelin. The charged lipids, hydrophilic surfactant protein SP-A, hydrophobic surfactant proteins SP-B and SP-C, and Ca^{2+} in the aqueous phase appear to contribute to the rapid spreading of the monolayer from its precursor material [1, 3, 25, 29, 30, 45, 46].

It is still not clear how the surfactant proteins specifically participate in the transformation of lamellar body material into an effective surfactant monolayer. Reorganization of the surfactant material on this scale is a very interesting manifestation of

lipid-protein interaction. Studies aimed at probing this interaction through the effect of the surfactant proteins on bilayer properties have been carried out using a variety of techniques including Raman and infrared spectroscopy [47–49], fluorescence studies [36, 37], differential scanning calorimetry (DSC) [50, 51], electron spin resonance (ESR) [46, 52], rhomboid surface balance [33, 34], epifluoresence microscopy [32], and ^{2}H-NMR spectroscopy [10, 12, 31, 51, 53, 54]. In this section, previous ^{2}H-NMR studies of phospholipid/surfactant protein interactions are reviewed.

In liquid-crystal-phase multilamellar vesicles, the ^{2}H-NMR spectrum of a chain deuteron is an axially symmetric Pake doublet split by an amount that depends on the extent to which the interaction between the nuclear quadrupole moment and the electric field gradient of the bond is averaged by reorientation (^{2}H-NMR theory will be reviewed in detail in the next chapter). The orientational order parameter, S_{CD}, for an individual deuteron is given by [58]:

$$S_{CD} = \frac{1}{2} < (3\cos^2\Theta_{CD} - 1) >$$

where Θ_{CD} is the angle between the C-^{2}H bond and the bilayer normal, and the average is taken over conformations sampled by the molecule as it reorients. For a chain-perdeuterated lipid, the weighted mean splitting, or first spectral moment (M_1), is proportional to the mean orientational order parameter for the chain. M_1 increases discontinuously at the liquid crystal to gel transition of a single component phospholipid bilayer and can thus be used to characterize bilayer phase behaviour as well as the perturbation of chain order by protein within the gel or liquid-crystalline phase.

In ^{2}H-NMR studies, a quadrupole echo sequence is usually used. The characteristic time for the decay of the quadrupole echo with increasing pulse separation is the transverse relaxation time, T_{2e}. This decay is sensitive to motions that reorient the

chain segment or the whole molecule on a time scale comparable with the inverse of the spectral width ($\sim 10^{-5}$ s). Such motions might include slow conformational changes in the molecule, the collective motion of the bilayer as a whole, and diffusion of the molecule along a curved bilayer surface [59]. Such slow motions appear to be particularly sensitive to the association of protein with the bilayer [60].

^{2}H-NMR has been used to study the effect of porcine SP-C protein on phase behaviour and on the chain orientational order of chain-perdeuterated DMPC (DMPC-d_{54}) [51]. It was found that, at a concentration of 8% (w/w), SP-C had no noticeable effect on acyl chain orientational order in the liquid-crystalline phase. The phase change from liquid crystal to gel was found to proceed continuously at this SP-C concentration. The gel-phase order, as indicated by first spectral moments, was found to be lower in the presence of SP-C. The protein had no significant effect on the spin-lattice relaxation of chain deuterons, which was taken as an indication that SP-C did not perturb the conformational changes on the time scale of the inverse Larmor frequency ($10^{-8} - 10^{-7}$s). SP-C was also found to lower the transverse relaxation time in the liquid-crystalline phase and flatten the temperature-dependence of the transverse relaxation time in the gel phase.

Dico *et al.* [53] have studied the effect of SP-C on the bilayer properties in binary mixtures of DPPC/DPPG bilayers, and in the corresponding single lipid DPPC and DPPG bilayers. SP-C was found to have a similar effect on the chain order and phase behaviour of phospholipid bilayers with a single lipid component. In gel phase DPPC/DPPG (7:3) bilayers with one or the other lipid component chain perdeuterated, SP-C was found to affect the first spectral moment more strongly for DPPG-d_{62} than for DPPC-d_{62}, which was attributed to SP-C having some preferential interaction with the negatively charged lipid DPPG. SP-C, in the absence of Ca^{2+}, was also found in this study to influence motions responsible for deuteron transverse relaxation

time in both the gel and liquid-crystalline phase. In the gel phase, Ca^{2+} appeared to remove the ability of SP-C to influence transverse relaxation. Another study focused on the perturbation of phospholipid headgroup conformation by SP-C. Morrow *et al.* [12] found that the addition of SP-C to the bilayer of DPPC deuterated at the α and β positions of the choline headgroup (DPPC-d_4) decreases α deuteron quadrupole splitting and, to a much lesser extent, increases β splitting. By comparison with previous results [55, 56], the authors [12] attributed this to the tilting of the headgroup dipole away from the the bilayer surface. It has been also demonstrated that α splitting was significantly more sensitive to changes in SP-C concentration than was β splitting. This was taken as a reflection of competition between charge-induced headgroup tilt and a change in the $\alpha - \beta$ torsional angle in responce to a change in steric constraints in the headgroup region of the bilayer [12].

The effect of pulmonary surfactant-associated protein SP-B on phospholipid bilayer properties has also been studied using ^{2}H-NMR spectroscopy [10, 54]. Synthetic SP-B was found to slightly increase acyl chain orientational order in liquid-crystalline phase DPPC-d_{62} bilayers, while its effect on gel phase chain order was neglegible [10]. As in the case of synthetic SP-B in DPPC-d_{62} [10], porcine SP-B, for concentrations up to 10%(w/w), was found to have little effect on acyl chain orientational order in liquid-crystaline phase DPPG-d_{62} and DPPC/DPPG-d_{62} (7:3) bilayers [54]. SP-B was also found to strongly perturb chain deuteron transverse relaxation in the liquid crystaline and gel phases of DPPC/DPPG-d_{62} (7:3) [54].

A series of experiments in a recent study have examined the orientational order and dynamics of deuterium-labeled phospholipids having SP-A and SP-B that display some tubular myelin organization [31]. This study showed that the liquid-crystalline to gel phase transition in a DPPC-d_{62}/egg-PG/SP-A/SP-B mixture occurs at a slightly lower temperature and is slightly broadened than in DPPC-d_{62} alone.

The transition remains relatively sharp for both DPPC-d_{62}/egg-PG/SP-A/SP-B and DPPC-d_{62}/SP-A/SP-B mixtures which is consistent with the previously reported effect of SP-B, at concentrations up to about 11%(w/w), on the transition [54]. This contrasts with the continuous phase change that was found in bilayers containing SP-C [60]. For both of the protein-lipid mixtures mentioned above, echo decay times in the liquid-crystalline phase were found to be significantly shorter than in the absence of protein [31]. While Dico *et al.* [54] have shown that the SP-B in DPPC/DPPG (7:3) interacts similarly with PC and PG, observations of DPPC/PG/SP-A/SP-B mixtures hydrated in the presence of Ca^{2+} suggested a stronger interaction of protein with PG than with PC [31].

Taken together, these ^{2}H-NMR results show that the hydrophobic proteins SP-B and SP-C have no significant effect on chain orientational order in the liquid-crystalline phase of phospholipid bilayers. Both proteins lower transverse relaxation time, T_{2e}, in both the liquid crystal and gel phases. The observation that in the liquid crystalline-phase the hydrophobic proteins reduce T_{2e} without effecting M_1 indicates that these proteins influence slow lipid motions.

1.3 Objective of this Work

The interaction of surfactant proteins with DPPC has been studied in phospholipids mixtures that display some tubular organization and in subsets of those mixtures. Electron microscopic studies by Suzuki *et al.* [29] and by Williams *et al.* [30] have shown that SP-A and SP-B, in the presence of Ca^{2+}, interact with DPPC/egg-PG bilayer to form tubular myelin structure. The presence of only one of these proteins was not sufficient for tubular myelin formation. Recent ^{2}H-NMR experiments [31] have studied the interaction of surfactant proteins SP-A and SP-B with DPPC/egg-

PG bilayer. This study focused on the effect of SP-A and SP-B together, in the presence of Ca^{2+}, on the DPPC/egg-PG bilayer properties. The present work is focused on the effect of SP-A alone, in the presence of Ca^{2+}, on the properties of DPPC/egg-PG bilayers. In this work, we address the following questions:

- How does the hydrophilic protein SP-A perturb bilayer order, phase behaviour and dynamics ?
- Does SP-A have an effect on the way in which SP-B interacts with the bilayer ?

To address these questions, the interaction of SP-A protein with DPPC/egg-PG bilayers was investigated in the gel and liquid-crystalline phase by using ^{2}H-NMR spectroscopy of chain and choline deuterated DPPC. The protein-lipid interaction is probed by means of observable ^{2}H-NMR parameters which are sensitive to molecular motions and reorientations. One of the studies described examines how SP-A, in the presence of Ca^{2+} ions and with or without SP-B, affects the orientational order, phase behaviour and dynamics of the acyl chains of DPPC. The second study looks at how SP-A interacts with the bilayer headgroup region. Based on the results, we ask how and where this protein interacts with the bilayer.

Chapter 2

^{2}H-NMR Theory

Bilayers of pulmonary surfactant, a complex mixture of lipids and proteins, are an example of a partially ordered system. In such systems, the molecular motions are generally anisotropic. The orientation dependent interactions, such as anisotropic chemical shift, dipole - dipole and quadrupole interactions are only partially averaged by the motions. Any external effect, such as temperature or addition of other components to the system, which may induce a change in the molecular motions can be detected by probing the relevant interactions by means of solid state NMR. ^{2}H-NMR is one method which has provided some powerful tools for the study of partially ordered systems [58–72]. This chapter treats the fundamental theory behind ^{2}H-NMR spectroscopy. The theory underlying the splitting of the Zeeman energy levels by the quadrupole interaction is first developed in the absence of the molecular motions. The expression of the quadrupole splitting is then expanded to account for motions which modulate the spectrum. The quadrupole echo and techniques for extracting structural and dynamic properties are briefly reviewed here.

The principle of NMR can be described briefly as follows. Atomic nuclei with intrinsic spin have a magnetic moment. In the presence of a magnetic field the nuclear

magnetization precesses about that field with frequency that depends upon magnetic field and the magnetic moment of the nucleus. Application of a current oscillating at this characteristic frequency to a coil oriented perpendicular to the applied field can tip the nuclear magnetization away from the applied field. If the duration of this radio-frequency pulse is selected to leave the nuclear magnetization precessing in the plane perpendicular to the applied field, the precessing magnetization can be detected via the oscillating voltage induced in the coil. This effect is called nuclear magnetic resonance and information about the environment of the nuclear spin is obtained from the perturbation of the precession frequency. For a spin-1 nucleus, such as deuterium, the precession is perturbed by the orientation-dependent quadrupole interaction. Information about the motion of the deuterated molecule is obtained from the extent to which this interaction is averaged by that motion.

2.1 The Electric Quadrupole Interaction

In deuterium NMR (^{2}H-NMR) experiments, a hydrogen atom can be substituted by a deuterium atom in a number of organic molecules being studied without changing the chemical and biochemical properties of the compound. The ^{2}H nucleus possesses spin angular moment I=1 and a small electric quadrupole moment Q= +2.875 x 10^{-3} barns [57].

The total Hamiltonian of a spin-1 system in a magnetic field can be generally written as

$$\mathcal{H} = \mathcal{H}_Z + \mathcal{H}_Q + \mathcal{H}_D + \mathcal{H}_C \tag{2.1}$$

where $\mathcal{H}_Z$ is the Zeeman interaction, $\mathcal{H}_Q$ is the quadrupole interaction, $\mathcal{H}_D$ is the dipolar interaction, and $\mathcal{H}_C$ is the chemical shift interaction. The dipolar and chemical interactions are much smaller than quadrupole interaction, and it is thus possible to

neglect them and treat the ^{2}H nucleus as an isolated spin-1 nucleus. Moreover, the electric quadrupole moment is small enough that the quadrupole interaction can be treated as a first order perturbation on Zeeman interaction in a magnetic field (3.5 T and 9.4 T in our lab.).

The Hamiltonian of Equation (2.1) then reduces to

$$\mathcal{H} = \mathcal{H}_Z + \mathcal{H}_Q. \tag{2.2}$$

The Zeeman interaction describes the interaction of the nuclear magnetic moment $\vec{\mu}$ with magnetic field $\mathbf{H}_o$. Consider an ensemble of N deuterons in a magnetic field $\mathbf{H}_o \| \ Z$. In the absence of any electric field gradient at the nucleus, the Zeeman interaction splits the ground state nuclear energy levels of the system as shown in figure 2.1. The Zeeman Hamiltonian in this case is

$$\mathcal{H}_Z = \vec{\mu} \cdot \mathbf{H_o} = -\gamma\hbar\omega_o \mathbf{I}_z. \tag{2.3}$$

where γ is the gyromagnetic ratio, ω_o ($= \gamma$ H$_o$) is the Larmor frequency and $\mathbf{I}_Z$ is the z-component of the spin angular moment. The allowed values of $\mathbf{I_z}$ are $m = -1, 0, 1$, and the energy of the interaction is

$$E_m = -m\hbar\omega_o. \tag{2.4}$$

For a nucleus with an electric quadrupole moment, as is the case for the deuterium nucleus, an electric field gradient, eq, at the site of the nucleus results in a shift of these nuclear Zeeman energy levels [61]. The electric field gradient arises from the electronic charge distribution of the atom or molecule containing the nucleus. If we use $V(\vec{r})$ for the potential due to this charge distribution and $\rho(\vec{r})$ for the nuclear charge distribution, the energy E of the interaction of the nucleus with its surrounding electric charge, can be written as [61]

$$E = \int \rho(\vec{r})\, V(\vec{r})\, d^3\vec{r} \tag{2.5}$$

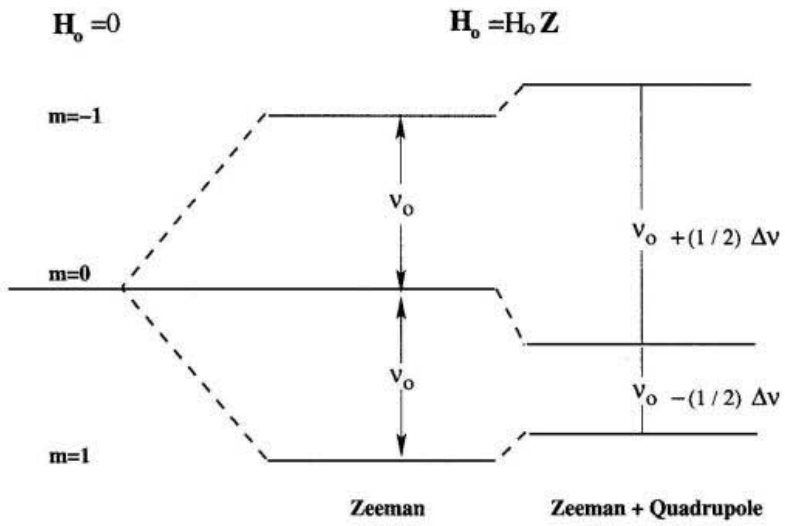

Figure 2.1: Splitting of the Zeeman energy levels by the quadrupole interaction.

where the integral is over the nuclear volume.

Starting with equation (2.5), the shift of the Zeeman energy levels can be evaluated by expanding the electric potential $V(\vec{r})$ in a Taylor's series. It can be shown, then, that the electric quadrupole interaction energy is given by [61, 62]

$$E^Q = \frac{1}{2}\sum_{\alpha\beta} V_{\alpha\beta} \int x_\alpha x_\beta \rho(\vec{r}) d^3\vec{r}. \tag{2.6}$$

where x_α ($\alpha = 1, 2, 3$) stands for x, y, or z respectively. The quantity

$$V_{\alpha\beta} = \frac{\partial^2 V}{\partial x_\alpha \partial x_\beta})_{\vec{r}=0} \tag{2.7}$$

is a symmetric traceless second order tensor, called the electric field gradient (EFG) tensor.

Utilizing the definition of the quadrupole moment

$$Q_{\alpha\beta} = \int (3x_\alpha x_\beta - \delta_{\alpha\beta} r^2)\rho(\vec{r}) d^3\vec{r} \tag{2.8}$$

the electric quadrupole interaction energy is thus given by [61, 62]

$$E^Q = \frac{1}{6}\sum_{\alpha\beta} V_{\alpha\beta} Q_{\alpha\beta}. \tag{2.9}$$

We have, then, a quadrupole term for the Hamiltonian $\mathcal{H}_Q$ given by the scalar product of EFG tensor with the quadrupole moment tensor. Different formulations of this product are possible, the most convenient being [62]

$$\mathcal{H}_Q = \frac{eQ}{6I(2I-1)} \sum_{\alpha\beta} V_{\alpha\beta}[\frac{3}{2}(I_\alpha I_\beta + I_\beta I_\alpha) - \delta_{\alpha\beta} I^2] \tag{2.10}$$

where I is the spin angular momentum. This quadrupole Hamiltonian can be expressed in the principal axes system of the EFG tensor. Since the electric field gradient has a preferential direction, it is appropriate to introduce an asymmetry parameter

$$\eta = \frac{V_{xx} - V_{yy}}{V_{zz}}$$

reflecting the relative contribution of the diagonal elements V_{xx}, V_{yy}, V_{zz} of the EFG tensor. Then the quadrupole Hamiltonian is [61, 62]

$$\mathcal{H}_Q = \frac{e^2qQ}{4I(2I-1)}[(3I_z^2 - I^2) + \eta(I_x^2 - I_y^2)]. \tag{2.11}$$

The principal axes system of the electric field gradient need not coincide with the laboratory system defined by the direction of the magnetic field $\mathbf{H}_0$. Thus, in order to see the effect of this Hamiltonian on the Zeeman energy levels, we must make a transformation of EFG from its principal axes system to the laboratory frame. This is conveniently done using the Wigner rotation matrix in the spherical coordinate system, to get the Hamiltonian in the laboratory frame as [58]

$$\mathcal{H}_Q = \frac{e^2qQ}{8I(2I-1)}[(3I_z^2 - I(I+1)][(3\cos^2\beta - 1) + \eta\sin^2\beta\cos 2\alpha] \tag{2.12}$$

so that, to first order, the quadrupole interaction shifts the Zeeman energy levels by the amount

$$E_m^Q = \frac{e^2qQ}{8I(2I-1)}[(3m^2 - 2)][(3\cos^2\beta - 1) + \eta\sin^2\beta\cos 2\alpha] \tag{2.13}$$

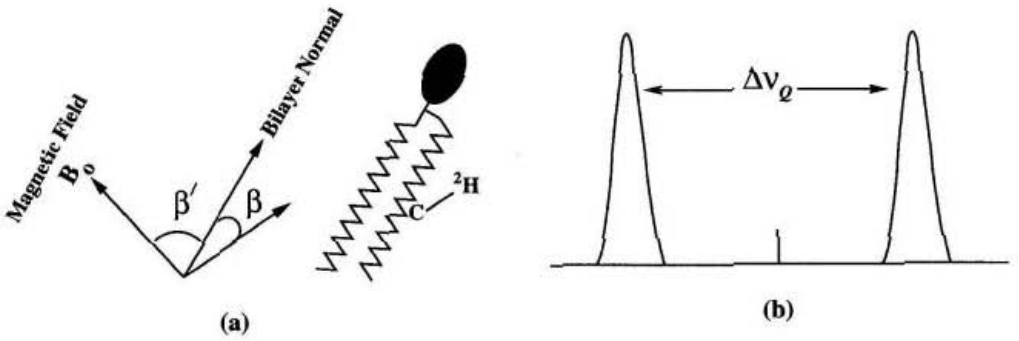

Figure 2.2: (a) C-^{2}H bond orientation and (b) splitting for single deuteron.

where the Euler angles α and β specify the orientation of the EFG principal axes in the laboratory frame. As a result, the energy levels corresponding to $m = \pm 1$ are shifted upward by an amount

$$\triangle = \frac{e^2qQ}{8}[(3\cos^2\beta - 1) + \eta\sin^2\beta\cos 2\alpha] \tag{2.14}$$

and the energy level corresponding to $m = 0$ is shifted downward by an amount $2\triangle$. The shifted levels are shown in figure 2.1 (right). The resultant energy level diagram consists of two allowed transitions. Instead of observing a singlet at frequency ν_0, we now observe a doublet which is symmetrically displaced about ν_0 with quadrupole splitting of [58, 61]

$$\triangle\nu_Q = \frac{3e^2qQ}{4h}[(3\cos^2\beta - 1) + \eta\sin^2\beta\cos 2\alpha] \tag{2.15}$$

as shown in figure 2.2(b). The quantity $e^2qQ\ /h$ is generally referred to as the *static quadrupole coupling constant.* For deuterons in C-^{2}H bonds it is roughly 169 kHz [63].

2.2 ^{2}H Quadrupolar Hamiltonian in the presence of Molecular Motion

In the previous section, the energy levels and quadrupole splittings have been derived for localized carbon-deuterium bond. However, in the presence of molecular motion, the quadrupole splittings are modulated by the molecular motion. To obtain the expression for this case, it is necessary to make the transformation from the molecule fixed principal axes frame to the laboratory system. We first transform from principal axes frame to the bilayer fixed frame and then from the bilayer fixed frame to the laboratory frame. In phospholipid bilayers, the bilayer normal is an axis of symmetry for molecular motion. The bilayer fixed frame is introduced such that the effect of molecular motion can be taken into account. In this case, α, β, and γ can be chosen to specify the Euler angles which transform from the principal axes frame to the bilayer fixed frame and α', β', and γ' to specify the Euler angles for transformation from the bilayer fixed frame to the laboratory frame. The symmetry of the molecular motion and that of the laboratory frame leaves α', γ', and γ arbitrary and they can be set to zero [58, 61]. Making use of this, it can be shown that the quadrupole splitting in the presence of molecular motion takes the form [58]

$$\triangle\nu_Q = \frac{3e^2qQ}{8h}(3\cos^2\beta' - 1) < [(3\cos^2\beta - 1) + \eta\sin^2\beta\cos 2\alpha] > \qquad (2.16)$$

where $< \cdots >$ indicates a time average. The time average is taken because the molecular reorientation may cause α and β to be time dependent. The angle β', defining the orientation of the molecular frame with respect to the laboratory frame of reference, may often be taken as fixed. Figure 2.2(a) defines the orientation of the molecular principal axes and molecular fixed frame with respect to the magnetic field (laboratory frame).

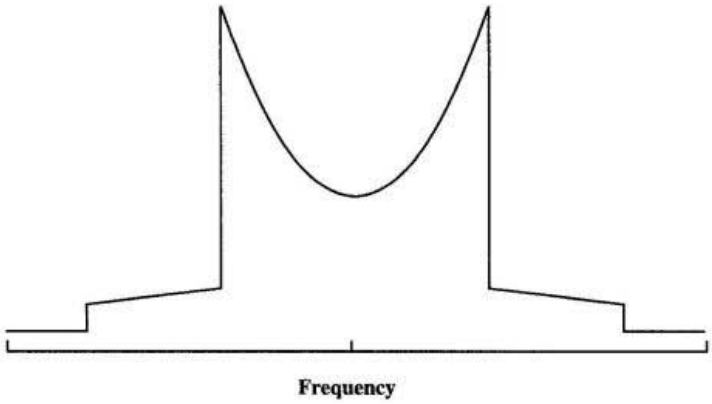

Figure 2.3: Model powder spectrum for phospholipids deuterated in a single acyl chain position. The sharp shoulders and peaks of the spectrum are broadened in real systems. The vertical axis is intensity.

The above analysis assumes that the NMR sample being studied is a homogeneously-oriented sample where all deuteron sites have the same orientation with respect to the magnetic field, or the electric field gradient tensor has the same orientation for all deuterium nuclei. In practical situations, the orientation of the molecular frame relative to the laboratory frame is not the same for all deuterons in a given sample. That is, the C-^{2}H bond vectors are not aligned parallel to each other and the orientation of the electric field gradient principal axes system is random. Such a sample is normally referred to as "powder" sample. In this case, the angle β' is not fixed, but takes all values. The different quadrupole splitting for C-^{2}H bonds having different orientations with respect to the magnetic field result in a powder spectral line shape similar to that shown in figure 2.3.

For the special case of an axially symmetric field gradient which has $\eta = 0$, the quadrupole splitting is [58]

$$\Delta\nu_Q = \frac{3e^2qQ}{8h}(3\cos^2\beta' - 1) < (3\cos^2\beta - 1) > . \qquad (2.17)$$

This is approximately true for the C-^{2}H bonds in the lipid acyl chain where η is very small [58, 63]. The quadrupole splitting is often written in terms of the orientational order parameter (S_{CD}, where D is for ^{2}H) as

$$\triangle\nu_Q = \frac{3e^2qQ}{4h}(3\cos^2\beta' - 1)S_{CD} \tag{2.18}$$

where S_{CD} is defined by [58]

$$S_{CD} = \frac{1}{2} < (3\cos^2\beta - 1) > . \tag{2.19}$$

When using ^{2}H-NMR for the study of ordered, anisotropic systems in the presence of molecular motion, one often deals with the average order parameter over all deuterated sites ($< S_{CD} >$) which is sensitive to the phase of the sample.

In dealing with perdeuterated samples, the method of moments is often used to extract information from a ^{2}H-NMR spectrum. For symmetric line shapes, like the one shown in figure 2.3, the nth spectral moments of the half spectrum is described by [58]

$$M_n = \frac{\int_0^\infty f(\omega)\omega^n d\omega}{\int_0^\infty f(\omega)d\omega} \tag{2.20}$$

where $f(\omega)$ is the spectral intensity as a function of frequency.

The first spectral moment (M_1) is directly related to mean quadrupole splitting (or equivalently the mean orientational order) by [58]

$$M_1 = (4\pi/3\sqrt{3}) < \triangle\nu_Q >= \frac{\pi}{\sqrt{3}}\frac{e^2qQ}{h} < S_{CD} > . \tag{2.21}$$

The second spectral moment(M_2) is also related to the splitting by [58]

$$M_2 = (4\pi^2/5) < (\triangle\nu_Q)^2 > . \tag{2.22}$$

By obtaining M_1 directly from a ^{2}H-NMR spectrum, the mean quadrupole splitting can easily be obtained. M_2 gives the mean square quadrupole splitting. Since M_1 is

directly proportional to $< S_{CD} >$, it is useful in studying the orientational order and phase transition which may affect this order parameter.

In the present work, the quadrupole echo technique, described below, is used to obtain the NMR signal or the free induction decay (FID). ^{2}H NMR spectra were obtained by Fourier transformation of the FID from which S_{CD} was extracted. FID will be discussed in more detail in a later section.

2.3 The Quadrupole Echo

The NMR pulse sequence used in all experiments described hereafter is the *quadrupole echo* [64]. It consists of two radio frequency (rf) pulses, separated by a time τ and shifted in phase by $\pi/2$ as illustrated in figure 2.4. The quadrupole echo technique was invented to avoid the problem of the dead time associated with receiver of the spectrometer [61, 64, 65]. For high rf coil ($Q \geq 10^2$), for example, it takes several microseconds for the signal due to a strong RF pulse to ring down to the noise level. During this time the NMR signal is obscured by the ring down of the probe and cannot be observed. Lowering the Q of the coil to shorten this dead time also reduces the sensitivity of the circut, and in biological membranes the signal-to-noise ratio often is quite low. At the same time, the initial part of the signal contains valuable information about the lineshape and ignoring this part of the signal would cause spectral distortion.

A solution to this problem for a spin-1 system can be achieved by applying a second pulse at time $t = \tau$ after the first pulse. Between the two pulses, the spin system dephases and evolves freely for time $t = \tau$. At time $t = \tau$ after the second pulse, the refocusing of all nuclear spins occurs and an echo is formed at time $t = 2\tau$ after the first pulse as illustrated in figure 2.4. If the pulse separation τ is chosen such

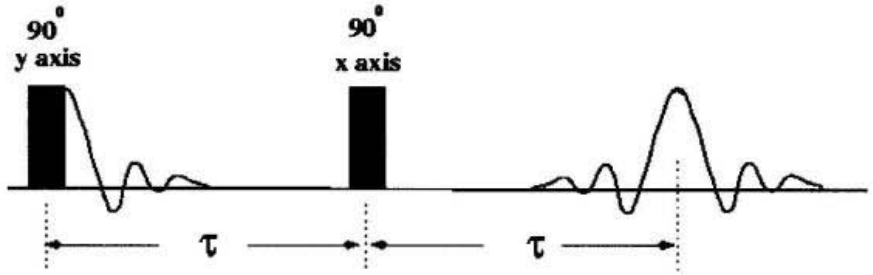

Figure 2.4: Quadrupole echo pulse sequence and the echo formation.

that the echo will occur after the receiver dead time, undistorted ^{2}H-NMR spectrum can be obtained. The amplitude of the echo observed at time 2τ depends on the molecular motions present during this time. Therefore, the echo amplitude decreases with increasing pulse separation. The characteristic time for the echo decay is labeled T_{2e}, the effective transverse relaxation time. This can be used as a parameter, as will be discussed later, to study the effect of external factors, such as temperature and/or addition of protein which influence the molecular motions [60].

2.3.1 Quadrupole Echo Formation

The quantum mechanical treatment for the quadrupole echo is conveniently done in terms of the evolution of the density matrix [61, 64, 65] following the two pulses. For spin-1 system ($I = 1$) the time-dependent density matrix is expressed in terms of nine ($(2I+1)^2$) 3×3 matrices in an operator space. One particular choice, in the rotating frame, is [61, 64]

$$\begin{gathered}
\mathbf{O_0 = 1} \qquad \mathbf{O_1} = \tfrac{1}{\sqrt{2}}\mathbf{I_x} \qquad \mathbf{O_2} = \tfrac{1}{\sqrt{2}}\mathbf{I_y} \qquad \mathbf{O_3} = \tfrac{1}{\sqrt{2}}\mathbf{I_z} \\
\mathbf{O_4} = \tfrac{1}{\sqrt{6}}(3\mathbf{I_z}^2 - 2\mathbf{1}) \qquad \mathbf{O_5} = \tfrac{1}{\sqrt{2}}(\mathbf{I_x I_z} + \mathbf{I_z I_x}) \qquad \mathbf{O_6} = \tfrac{1}{\sqrt{2}}(\mathbf{I_y I_z} + \mathbf{I_z I_y}) \\
\mathbf{O_7} = \tfrac{1}{\sqrt{2}}(\mathbf{I_z}^2 - \mathbf{I_x}^2) \qquad \mathbf{O_8} = \tfrac{1}{\sqrt{2}}(\mathbf{I_x I_y} + \mathbf{I_y I_x}).
\end{gathered} \tag{2.23}$$

Following the notation of Davis [61], the axially symmetric part of the quadrupolar

Hamiltonian given by Equation (2.12) can be written in terms of these operators as

$$\mathcal{H}_Q = \frac{1}{3}\omega_Q(3I_z^2 - 2) = \sqrt{\frac{2}{3}}\hbar\omega_Q\mathbf{O_4} \tag{2.24}$$

and the Hamiltonian during the first 90^0 pulse of strength ω_1, along the y-axis, is

$$\mathcal{H}_y = -\sqrt{2}\hbar\omega_1\mathbf{O_2}. \tag{2.25}$$

The initial state of a spin system considered here is that of an ensemble of N deuteron nuclei allowed to come to thermal equilibrium with the lattice at temperature T in strong magnetic field, $\mathbf{H}_o$, oriented parallel to the z-axis. This state is described by the density matrix as

$$\rho(0) = \mathbf{1} + C_3(0)\mathbf{O_3} \tag{2.26}$$

where

$$C_3(0) = \hbar\omega_0/3k_\beta T \tag{2.27}$$

and all other coefficients are zero [66].

During the first 90^0 pulse of duration t_y and strength ω_1, along the y-axis, the system evolves under the Hamiltonian $\mathcal{H}_y$ given by Equation (2.25). During this first pulse, the only nonzero coefficients are C_1 and C_3. The time evolution of each is described by corresponding Liouville equations whose solutions are

$$\begin{aligned} C_1(t_y) &= (-\sqrt{2}\hbar\omega_0/3k_\beta T)\sin(\omega_1 t_y) \\ C_3(t_y) &= (-\sqrt{2}\hbar\omega_0/3k_\beta T)\cos(\omega_1 t_y). \end{aligned} \tag{2.28}$$

This pair of solutions describes precession of the vector magnetization about the component of the rf field in the rotating frame, or in operator space, the precession occurs in the $(\mathbf{O_1}, \mathbf{O_3})$ plane. For a pulse such that $\omega_1 t_y = \pi/2$, the z-component of the magnetization at the end of the rf pulse is rotated into the negative x-axis.

Right after the first pulse, the spin system is allowed to evolve for a time τ under the influence of the quadrupolar Hamiltonian given by Equation (2.24). The nonzero

coefficients during this time period are C_1 and C_6. The solution of their corresponding Liouville equations at time τ takes the form

$$\begin{aligned} C_1(\tau) &= (\sqrt{2}\hbar\omega_0/3k_\beta T)\cos(\omega_Q\tau)\sin(\omega_1 t_y) \\ C_6(\tau) &= (\sqrt{2}\hbar\omega_0/3k_\beta T)\sin(\omega_Q\tau)\sin(\omega_1 t_y). \end{aligned} \tag{2.29}$$

Now the precession, under the influence of the quadrupolar Hamiltonian, is in the $(\mathbf{O_1}, \mathbf{O_6})$ plane of operator space. In the spin space the quadrupolar Hamiltonian converts the $\mathbf{I_x}$ operator into a linear combination of $\mathbf{I_yI_z}$ and $\mathbf{I_zI_y}$.

The coil in a NMR experiment is perpendicular to the magnetic field $\mathbf{H}_o$ and can detect the transverse magnetization M_x and M_y. Thus, after the first 90^0 pulse the signal (in rotating frame) is $< M_x >$, which is proportional to $< I_x >$:

$$< I_x >= \sqrt{2}C_1 = (2\hbar\omega_0/3k_\beta T)\cos(\omega_Q\tau)\sin(\omega_1 t_y). \tag{2.30}$$

This is the signal at the beginning of the FID following the pulse.

A second pulse of duration $t = t_x$ and strength ω_2, this time applied along the x-axis, is used to form the quadrupolar echo, as shown in figure 2.4. After this second pulse the system is again allowed to evolve under the quadrupolar Hamiltonian (Equation 2.24). Only C_1 and C_6 are not zero and need to be examined. Again $\mathcal{H}_Q$ couples $\mathbf{O_1}$ to $\mathbf{O_6}$, but with different initial conditions following the two $\pi/2$ pulses:

$$C_1(\tau + t_x) = (\sqrt{2}\hbar\omega_0/3k_\beta T)\cos(\omega_Q\tau) \quad \text{and} \quad C_6(t_x) = (-\sqrt{2}\hbar\omega_0/3k_\beta T)\sin(\omega_Q\tau).$$

Finally, at time t' following the removal of the second pulse,

$$\begin{aligned} C_1(t) &= (\sqrt{2}\hbar\omega_0/3k_\beta T)\sin(\omega_Q\tau)\sin(\omega_Q t') + \cos(\omega_Q\tau)\cos(\omega_Q t') \\ C_6(t) &= (\sqrt{2}\hbar\omega_0/3k_\beta T)\sin(\omega_Q\tau)\cos(\omega_Q t') - \cos(\omega_Q\tau)\sin(\omega_Q t'). \end{aligned} \tag{2.31}$$

From the origin of the pulse sequence $t = t' + \tau$, neglecting t_x and t_y, the above equations become

$$\begin{aligned} C_1(t) &= (\sqrt{2}\hbar\omega_0/3k_\beta T)\cos(\omega_Q[t - 2\tau]) \\ C_6(t) &= (-\sqrt{2}\hbar\omega_0/3k_\beta T)\sin(\omega_Q[t - 2\tau]). \end{aligned} \tag{2.32}$$

The quadrupole signal can be obtained from the expression for C_1:

$$< I_x >= \sqrt{2}C_1 = (2\hbar\omega_0/3k_\beta T)\cos(\omega_Q[t-2\tau]). \tag{2.33}$$

The signal is symmetric about $t = 2\tau$ and has a maximum at this time. If relaxation is neglected, the amplitude is equal to the amplitude of the FID immediately following the first pulse. Quadrupole echo, in this way, recovers the FID completely in a time 2τ after the first pulse, well beyond the recovery time of the receiver and after the ringing of the transmitter has ended.

2.3.2 Molecular Motions and ^{2}H Quadrupolar Relaxation

The quadrupole echo sequence consists of two $\pi/2$ radio frequency pulses separated by an interval τ. The echo is formed at time 2τ following the start of the sequence. Molecular motions which alter the orientation-dependent quadrupole interaction during the interval 2τ contribute to the echo decay. As an example, figure 2.5 shows experimental data collected for DPPC-d_{62}/egg-PG bilayer at 55°C. Figure 2.5 shows the variation of quadrupolar echoes amplitude with the pulse spacing τ.

Some molecular motions that may lead to echo decay in both gel and liquid-crystalline phase bilayers include bilayer surface undulation [59], diffusion along curved surfaces [68], collective bilayer modes [69], intermolecular motions (such as chain fluctuation and molecular rotations) and intra-molecular motions (such as *trans-gauche* isomerization) [70]. A given motion, i, is characterized by a correlation time and the apparent second moment, ΔM_{2i}, of the quadrupolar Hamiltonian modulated by the motion. The order of the magnitude of the correlation time, τ_c, of these motions in the liquid-crystalline phase have been determined. The correlation time of bilayer undulation is of the order of 100 μs [59, 65], while that of the lateral diffusion is of the order of 100 ms [59]. The correlation time of the collective bilayer mode is also

of the order 10 μs. The correlation times of chain rotation and fluctuations motions are of the order of 10^{-8}s [70]. *Trans-gauche* isomerization occurs at a faster rate and its correlation time is of the order 10^{-10}s [70].

The limiting cases of fast and slow motions are defined in terms of the relationship between the correlation time for the motion, τ_c, and the reduction in the apparent second moment, ΔM_2, due to the motion [67]. ΔM_2 is given by

$$\Delta M_2 = M_2 - M_{2r} \tag{2.34}$$

where M_2 is a full second moment of the interaction and M_{2r} is the residual second moment (that is the second moment of the motionally narrowed spectrum). For fast motion, the correlation times are related to ΔM_2 by $\Delta M_2 \cdot \tau_c^2 \ll 1$, while those for the slow motion are related by $\Delta M_2 \cdot \tau_c^2 \gg 1$.

The quadrupolar relaxation is characterized by the effective transverse relaxation time, T_{2e}, the inverse of the transverse relaxation rate averaged over all deuterons in a given sample. For fast motion, which contributes to motional narrowing, the general theory of motional averaging gives [67, 68]

$$\frac{1}{T_{2e}} = \Delta M_2 \cdot \tau_c \tag{2.35}$$

while for slow motion, which does not contribute to motional narrowing, T_{2e} is given by

$$T_{2e} = p \cdot \tau_c \tag{2.36}$$

where $p \geq 1$.

For fast motions $T_{2e} \propto \tau_c^{-1}$ while for slow motions $T_{2e} \propto \tau_c$. Therefore, in the intermediate motion situation, $\Delta M_2 \cdot \tau_c^2 \approx 1$, and T_{2e} must go through a minimum. Pauls *et al.* [67] propose, for the region of intermediate τ_c, an expression of the form

$$\frac{1}{T_{2e}} = \frac{\Delta M_2 \cdot \tau_c}{1 + p\Delta M_2 \cdot \tau_c} \tag{2.37}$$

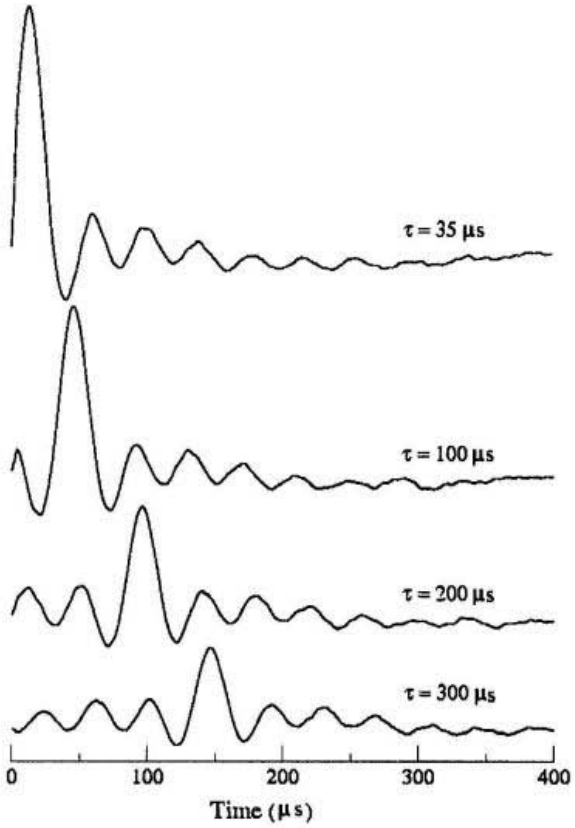

Figure 2.5: Quadrupolar echoes as a function of pulse spacing (τ).

which is reduced to expression (2.35) for short τ_c and (2.36) for long τ_c. At the minimum

$$T_{2e}(min) \approx \frac{2p}{\Delta M_2} \quad \text{and} \quad \tau_c \approx \sqrt{p\Delta M_2}. \tag{2.38}$$

In the liquid-crystalline phase, away from the main transition, slow motions such as bilayer surface undulation, lateral diffusion and collective lipid motions are significant contributors to relaxation. These motions are sensitive to the association of protein with bilayers [60]. As discussed above, for these motions T_{2e} is proportional to their correlation time. The chain fluctuations and molecular rotations are fast and their contribution to T_{2e} is inversely proportional to their correlation time. As temperature decreases the correlation times of chain fluctuations, molecular rotation

and *trans-gauche* isomerization motions increases so T_{2e} decreases. At the phase transition correlation times for these three motions are of the order of 10^{-6}s to 10^{-5}s [70]. Bilayer undulation, lateral diffusion and collective mode motions freeze out on the time scale of the quadrupole echo sequence and they do not affect T_{2e}. Just below the main phase transition, the correlation times of the remaining motions become comparable to the pulse separation so T_{2e} assumes a minimum. Further increase in the correlation times results in an increase in T_{2e} in the gel phase. In the gel phase the intermolecular motions likely freeze out on the experimental time scale and fast intra-molecular motions are expected to contribute mainly to the decay resulting in the observed T_{2e} maximum.

In chapter 4 results illustrate that the addition of the surfactant protein SP-A to a lipid bilayer induces changes in the correlation times of the motions of the bilayer which can be detected by ^{2}H transverse relaxation time (T_{2e}) measurements. This provides us with some information concerning the interaction of the protein with the bilayer.

Chapter 3

Experimental Setup and Details

3.1 ^{2}H-NMR Experimental Setup

All experiments in this work were performed on locally constructed solid state ^{2}H-NMR spectrometers, and using superconducting magnets with field strengths of 3.5 Tesla (Nalorac Cryogenic, Martinez, CA) and 9.4 Tesla (Magnex Scientific, Concord, CA). A block diagram of the 9.4 T NMR spectrometer is shown in figure 3.1.

The PTS-160 synthesizer (Programmed Test Sources Inc., Littleton, MA) provides signals with frequencies of 71.4 MHz and 10 MHz. The 10 MHz signal is fed into a phase splitter. Another 10 MHz signal is edited into pulses with phases of 0^o, 90^o, 180^o and 270^o in the pulse generator and then sent to mixers contained in the single side-band generator. The output and the duration (t_p) of these pulses are controlled by a home built pulse programmer. The 71.4 MHz signal is sent to both the single side-band generator and the receiver. Upon reaching the single side-band generator, the 71.4 MHz signal is mixed with the 10 MHz signal to generate pulses at the ^{2}H resonance frequency of 61.4 MHz. These pulses are then sent, via a pulse amplifier to a home built transmitter. The 1000 W LPI-10 amplifier (ENI, Rochchester, NY)

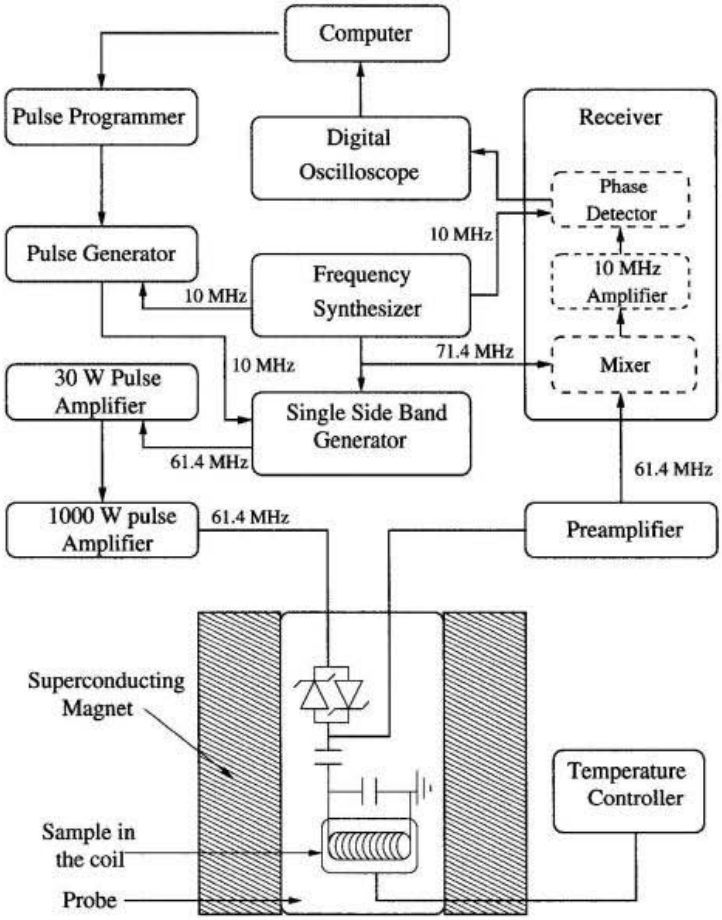

Figure 3.1: Block diagram of 9.4 T NMR spectrometer.

transmits pulses at the resonance frequency with an amplitude of about 300 V into the probe (rf coil). The pulse amplifier that was used in the 3.5 T NMR spectrometer was a Henry SS1200HF amplifier (Henry, Los Angeles, CA).

The response of the spin system to a pair of high power pulses induces a weak voltage signal in the coil. This weak signal is amplified in the preamplifier and then fed into the receiver system. The receiver system contains a mixer, a 10 MHz amplifier, and a quadrature detector. The mixer mixes the 71.4 MHz signal from the frequency synthesizer with the 61.4 MHz carries wave modulated by the FID signal from the

preamplifier and generates a 10 MHz carrier wave modulated by the FID signal. This is sent to the quadrature detector, which detects both the real and the imaginary parts of the FID signal separately by comparing the FID signal with the reference signal coming from the frequency synthesizer. The FID signals are then digitized by a digital oscilloscope with a desired sampling time.

3.2 Experimental Details

^{2}H NMR spectra were acquired using the quadrupole echo sequence described in section 2.3 with $\pi/2$ pulse lengths ranging from 4.5 - 5.5 μs. Upon instruction by the computer, the rf transmitter produces the short $\pi/2$ pulses which are channeled to the probe tank circuit. The probe resonantly excites the nuclei. Once the transmitter pulse has been removed the nuclear signal is free to pass to a low noise preamplifier and high gain receiver. The voltage generated by the receiver is then digitized and sent to the computer to be stored as the time domain signal. Quadrature detection and phase cycling were used to minimize errors due to instrumental imperfections [71]. Spectra acquired on the 9.4 T NMR system were obtained by averaging 20,000 transients (48,000 on the 3.5 T NMR system). In both cases, FID was obtained with phase cycling using a repetition time of 0.5 s. For samples containing chain-deuterated lipids, from which first spectral moments were taken, the $\pi/2$ pulses of the quadrupole echo sequence were typically separated by 35 μs and the FID decay was over sampled by a factor of four to give effective dwell times of 4 μs for both liquid-crystalline and gel phase samples [72]. Spectra of choline-deuterated lipids were obtained with $\pi/2$ pulse separation of 50 μs and on effective dwell times, after over sampling, of 5 μs. For transverse relaxation time measurements, pulse separations were varied from 35 μs to 300 μs. A Visual Basic program was employed to analyze the ^{2}H-NMR experiments

that were performed on the 9.4 T NMR system and a Turbo C program was used for those performed on the 3.5 T NMR system. Data were collected on a Celeron 433 MHz PC (for the 9.4 T NMR system) and on a 386 PC (for the 3.5 T NMR system).

A temperature controller was used to maintain constant temperature around the sample using thermocouples placed in the bore of the magnet. The sample tube and probe coil were enclosed within a copper oven, the temperature of which was maintained by the microprocessor-based temperature controller. Experiments were carried out for a series of temperatures beginning at 55 ^{o}C and descending in steps of 2 ^{o}C (1 ^{o}C near the phase transition). Cold nitrogen gas from evaporation of liquid nitrogen was blown over the sample where cooling below room temperature was desired. Samples were allowed to reach thermal equilibrium, before starting each experiment, by waiting for at least 60 minutes after each cooling step.

3.3 Sample Preparation

All the samples used in this work were prepared in Dr. K. M. W. Keough's laboratory (Biochemistry, Memorial University) by J. Stewart according to the following protocol.

Chain-perdeuterated dipalmitoylphosphotidylcholine (DPPC-d_{62}, DPPC-d_{31}) and choline-labled DPPC-d_4, along with egg-PG were purchased from Avanti Polar Lipids (Alabaster, AL). The phospholipids were analyzed for purity by thin-layer chromatography and were used without further purification.

Pulmonary surfactant proteins SP-A and SP-B were obtained from porcine lung lavage as previously described [31, 32]. SP-A was isolated by injecting a suspension of porcine surfactant into stirred 1-butanol for 30 minutes [32]. The mixtures were then centrifuged at 10000g for 20 minutes. The precipitate was dried under nitrogen and

washed twice in 20 ml of buffer (10 MHz HEPES/100 mM NaCl/20 mM n-octyl-β-D-glucopyranoside/PH 7.4). After centrifugation at 100000g, following each wash, for 30 minutes, the resulting material was suspended in small volume of 5 mM HEPES (PH 7.4), and dialyzed against 5 mM HEPES (PH 7.4) for 48 hours. The dialyzed material was then centrifuged at 100000g for 30 minutes and the supernatant, which contained the purified SP-A, was stored in small aliquots at -20 ^{0}C. SP-B was obtained from lipid extracts of porcine surfactant [31]. This was performed by gel exclusion chromatography on Sephadex LH-60 in 1:1 (v/v) chloroform/methanol containing 2% by volume 0.1 M HCl.

Samples for NMR observation were prepared as follows. To prepare sample containing lipids, SP-A, SP-B, the lipids and SP-B were first mixed in 1:1 (v/v) chloroform/methanol. This mixture was dried under a stream of nitrogen, evacuated overnight, and then hydrated in 10 ml of buffer (10 mM TRIS/145 mM NaCl/1 mM EDTA/ pH 7.4) at 46 ^{o}C for 1 hour. The sample was then centrifuged at 50000g for 30 minutes. The resulting pellet was resuspended in 1 ml of the supernatant, and the lipid concentration determined. SP-A, in buffer, was then added to give a final concentration in terms of total solid of 16% SP-A, 11% SP-B, and 73% lipids. After a short incubation at 37 ^{o}C, calcium was added to give a final concentration of 5 mM. Following overnight incubation at 37 ^{o}C, 500 μl was removed for electron microscopy. The remaining sample was centrifuged briefly in a bench-top centrifuge to obtain a pellet which was then scraped into an 8mm NMR tube. For samples containing only lipids and SP-A, the above procedure was followed to obtain samples with final concentration of 16% SP-A, and 84% lipids.

Samples for electron microscopy were fixed overnight at room temeprature in an equal volume of sodium cacodylate buffer (pH 7.4) containing 1% OsO_4 by weight. This fixative was replaced with 2% aqueous uranyl acetate and left overnight at 4^{o}C.

Samples were then dehydrated in increasing concentrations of acetone, from 70%-100% in 10% steps, and embedded in TAAB 812 resin. Sections were made and then stained with 5% uranyl acetate in 50% ethanol followed by 3-5% lead citrate in water. Sections were viewed using a Zeiss 109 electron microscope. This was done in Dr. K. M. W. Keough's laboratory (Biochemistry, Memorial University) by J. Stewart.

Chapter 4

Results and Discussion I: SP-A Effect on DPPC Acyl Chain

4.1 Introduction

SP-A is one of the essential components that play a major role in the conversion of the lamellar bodies into a surface active monolayer that lines the alveolar air-water interface. Tubular myelin is thought to act as a reservoir or precursor for the surface monolayer [1, 26, 28]. The generation of tubular myelin *in vitro* has been found to require the presence of SP-A, SP-B, DPPC, PG and calcium [29]. A recent study has shown that the DPPC-d_{62}/egg-PG mixtures containing SP-A and SP-B display a shift of intensity toward the center of their ^{2}H-NMR spectra [31]. This was attributed to an increase in the isotropic character of lipid motions resulting from the presence of proteins in the mixtures. In the work described in this chapter, effects of the hydrophilic SP-A protein on the DPPC/egg-PG bilayers are investigated. This is done by probing the effect of SP-A on the chain order, phase behaviour, and dynamics of chain-perdeuterated lipid in DPPC/egg-PG bilayers using ^{2}H-NMR.

4.2 Electron Microscopy Results

Figure 4.1 shows electron micrographs of some structures resulting from preparation protocols used to obtain the samples investigated by ^{2}H-NMR spectroscopy. Electron micrographs were provided by J. Stewart (Dr. Keough's laboratory, Biochemistry, Memorial University). Figure 4.1A shows a lipid-protein mixture comprising, by weight, 73% phospholipid (DPPC-d_{62}/egg-PG (7:3)), 16% SP-A and 11% SP-B hydrated in buffer containing 5 mM Ca^{2+} before being fixed. This section displays regions of multilamellar organization with layers uniformly separated by about 30 nm and square lattice regions, with edges of 30-35 nm, typical of tubular myelin organization. These modes of organization are similar to those reported by Williams *et al.* [30] for comparable mixtures of lipid and protein. Figure 4.1B is an electron micrograph of a section from a lipid-protein mixture comprising, by weight, 66% DPPC, 24% SP-A, and 10% SP-B hydrated in buffer containing 5 mM Ca^{2+}. This mixture lacks the unsaturated phosphatidylglycerol component that appears to be necessary for tubular myelin organization. Figure 4.1B shows regions of multilamellar organization with layers uniformly separated by about 25-30 nm. This separation is comparable to the dimensions of the SP-A head region, which associates with the membrane surface [22], and likely reflects the accommodation of at least part of the SP-A octadecamer between layers [30]. The absence of any evidence of tubular myelin organization, however, is consistent with reports that unsaturated PG is a necessary prerequisite for tubular myelin organization [29, 30]. Figure 4.1C is an electron micrograph of DPPC-d_{62}/egg-PG (7:3) hydrated in buffer containing 5 mM Ca^{2+}. The micrograph shows vesicles of widely varying size with little evidence of multilamellar organization. Williams *et al.* [30] obtained similar electron micrographs from protein-free lipid mixtures. Figure 4.1D shows an electron micrograph obtained from a lipid pro-

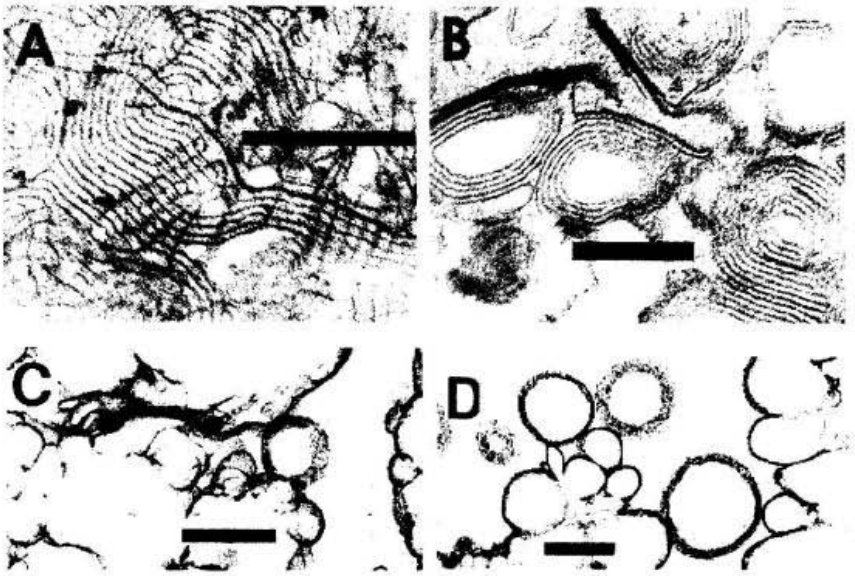

Figure 4.1: Electron micrographs of (A) 51% DPPC-d_{62}, 22% egg-PG, 16% SP-A and 11% SP-B, (B) 66% DPPC-d_{62}, 24% SP-A and 10% SP-B, (C) DPPC-d_{62}/egg-PG (7:3) and (D) DPPC-d_{62}/egg-PG (7:3) with 16% SP-B. All samples were hydrated in buffer containing 5 mM Ca^{2+}. Bars represent 500 nm.

tein mixture comprising DPPC-d_{62}/egg-PG (7:3) with 16% SP-B hydrated in buffer containing 5 mM Ca^{2+}. The dominant mode of organization is vesicular. There is no evidence of the 20-30 nm layer spacing characteristic of samples containing SP-A but there may be some multilamellar organization with layer separation below the resolution of the micrograph.

4.3 ^{2}H-NMR Results

Solid-state ^{2}H-NMR is one of several techniques that provide insight into the way the surfactant proteins interact with phospholipid bilayers. The effect of SP-A on

the physical properties of DPPC/egg-PG bilayers was studied by observing ^{2}H-NMR spectra and quadrupole echo decay rates as presented below.

4.3.1 ^{2}H-NMR Spectra and First Spectral Moment

A ^{2}H-NMR spectrum of fully-hydrated chain-perdeuterated phospholipids is a superposition of axially averaged powder patterns arising from the different deuterons for the various C-^{2}H segments along the acyl chains. For fluid bilayers the molecular motions are axially symmetric with respect to the bilayer. The quadrapole splitting of each powder pattern is given by equation 2.18:

$$\triangle\nu_Q = \frac{3e^2qQ}{4h}(3\cos^2\beta' - 1)S_{CD},$$

where

$$S_{CD} = \frac{1}{2} < (3\cos^2\beta - 1) > .$$

The angle β describes the orientation of the C-^{2}H bond with respect to the bilayer normal and β' is the angle between the bilayer normal and the static magnetic field as illustrated in figure 2.2. The deuteron order parameter S_{CD} reports on the average over the accessible chain conformations of the phospholipid molecule and the amplitude of the motions of the corresponding C-^{2}H bond. The mean orientational order parameter $< S_{CD} >$ is averaged over all deuteron sites in the sample being studied and thus provides time-averaged structural information about the bilayer.

For a chain-perdeuterated lipid, the weighted mean splitting, or first spectral moment, M_1, is directly related to $< S_{CD} >$ through

$$M_1 = \frac{\pi}{\sqrt{3}}\frac{e^2qQ}{h} < S_{CD} > .$$

M_1 increases discontinuously at the liquid crystal to gel transition of a single component phospholipid bilayer and can thus be used to characterize bilayer phase behaviour

as well as the perturbation of chain order by protein in the gel or liquid crystalline phase.

To study effects due to the presence of SP-A in DPPC/egg-PG bilayers, ^{2}H-NMR spectra were collected at selected temperatures. Figure 4.2 shows ^{2}H-NMR spectra for DPPC-d_{62}/egg-PG (7:3) and DPPC-d_{62}/egg-PG (7:3) containing 16% (w/w) SP-A both hydrated in buffer containing 5 mM Ca^{2+}. Figure 4.3 shows ^{2}H-NMR spectra at selected temperatures for DPPC-d_{62}/egg-PG (7:3) containing 16% (w/w) SP-A and 11% (w/w) SP-B hydrated in buffer containing 5 mM Ca^{2+}. In each figure the spectra illustrate that the bilayers go from the liquid crystalline phase, at the highest temperatures, to the gel phase at the lowest temperatures. In the absence of SP-A, in the liquid crystalline phase, spectra are superpositions of sharp doublets arising from fast axially symmetric reorientation of C-^{2}H bonds with respect to the bilayer normal. In the gel phase, the spectra are wider and have a more continuous intensity distribution which is indicative of hindered rotation. It is apparent that in the presence of SP-A the intensity of different splittings is affected. This may be related to the change in deuteron transverse relaxation time (T_{2e}). T_{2e} may not be uniform across the spectrum. For spectra of both samples in figure 4.2 the change from liquid crystalline to gel phase proceeds continuously. It has been reported previously that, for pure DPPC, a sharp transition from liquid crystalline to gel phase occurs at 37°C [10, 31]. The addition of egg-PG to the DPPC bilayer makes the transition proceed continuously (figure 4.2(*left*)). Taking this into account, the spectra suggest that the effect of PG on DPPC bilayers was not removed by SP-A and hence, there is no specific interaction for SP-A protein with either lipid component of the the mixture.

The results illustrated in figure 4.3 show that the addition of 11% (w/w) SP-B to DPPC-d_{62}/egg-PG bilayers containing 16% (w/w) SP-A makes the transition

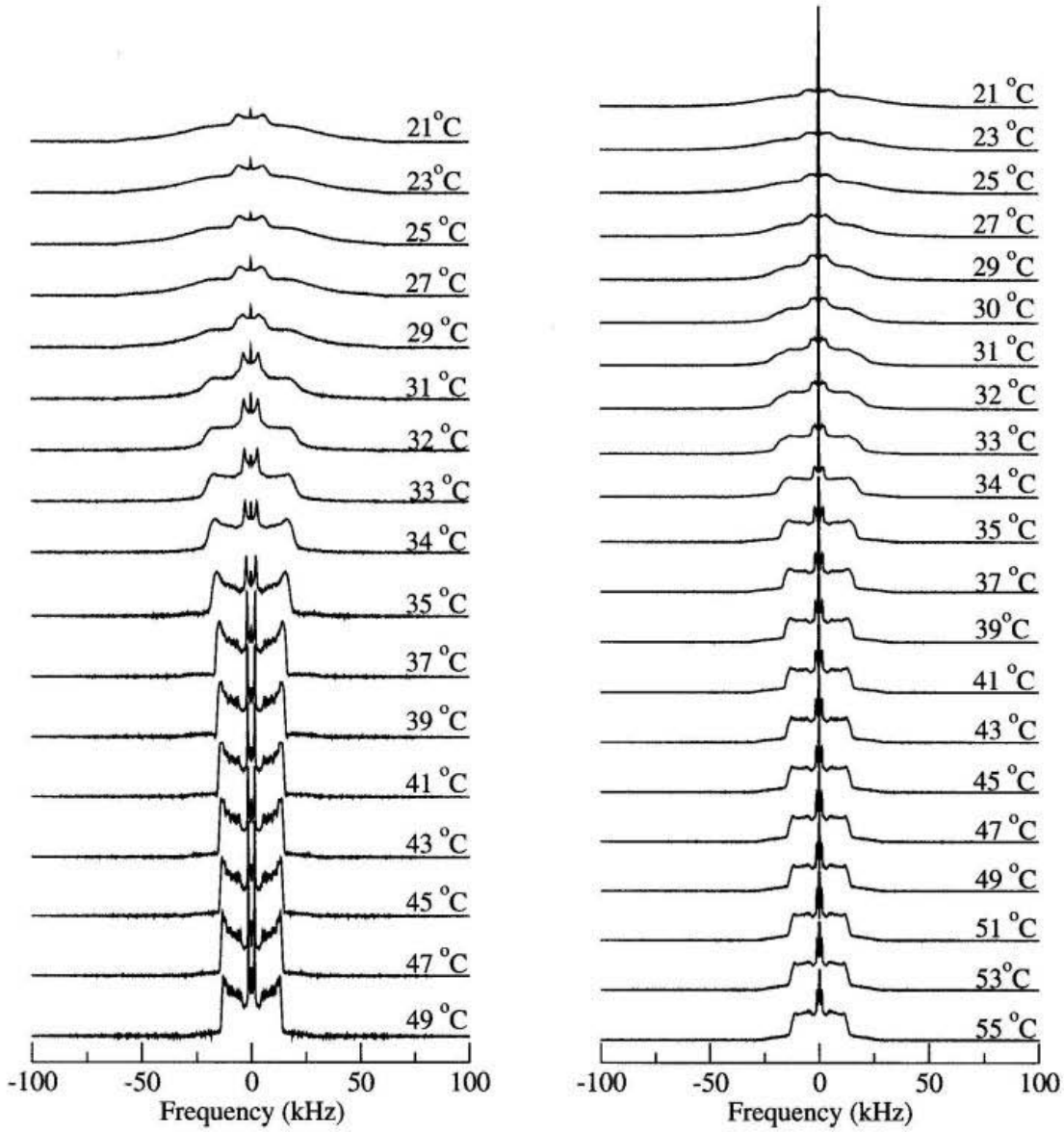

Figure 4.2: Temperature dependence of the ^{2}H-NMR spectrum of DPPC-d_{62}/egg-PG (7:3) bilayer (*left*) and a bilayer with 16% (w/w) SP–A (*right*). Both samples were hydrated in buffer containing 5 mM Ca^{2+} .

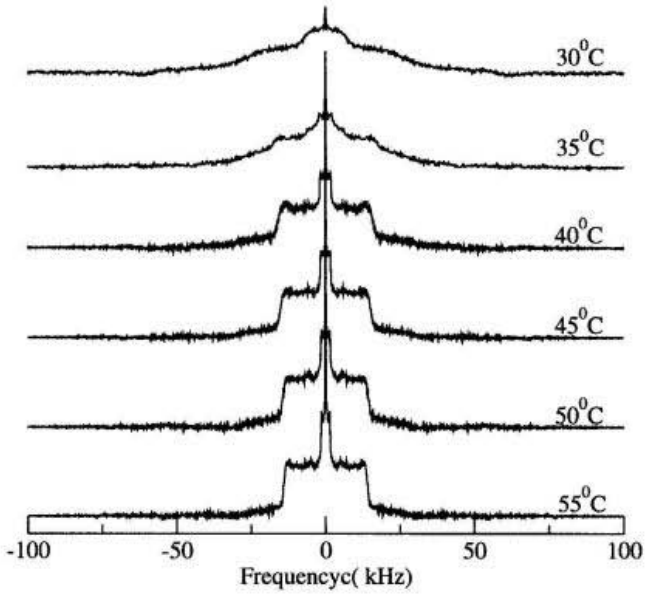

Figure 4.3: Temperature dependence of the ^{2}H-NMR spectrum of DPPC-d_{62}/egg-PG (7:3) bilayer with 16% (w/w) SP–A and 11% (w/w) SP–B hydrated in buffer containing 5 mM Ca^{2+}.

relatively sharp. An earlier ^{2}H-NMR study [10] has shown that DPPC-d_{62} bilayers containing 11% (w/w) SP-B display a relatively continuous change of spectral character from the liquid crystal to the gel phase. Comparing this with our results (Figures 4.2 and 4.3) suggests that SP-A and SP-B proteins work together to induce the sharp transition observed in figure 4.3. A possible explanation is that SP-A and SP-B interact in a specific way to remove the effect of PG on the DPPC bilayers. Because of the complexity of this sample in having two protein components, another explanation is possible. SP-B may have a preferential interaction with PG such that the effect of PG on DPPC bilayers has been removed without any contribution from SP-A.

As mentioned above, the ^{2}H first spectral moment (M_1) gives the mean quadrupole splitting or the mean orientational order parameter. M_1 was measured to study the effect of SP-A on the mean orientational order of acyl chains of deuterated lipid in

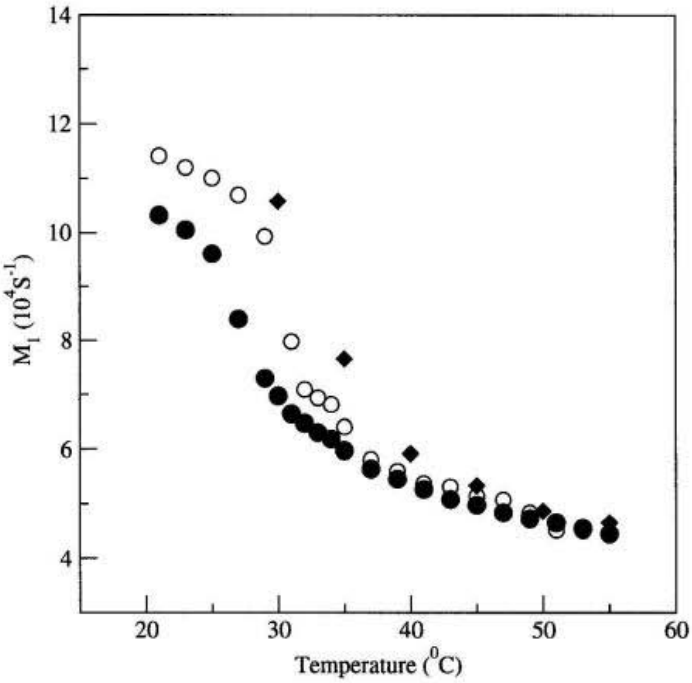

Figure 4.4: Temperature dependence of ^{2}H-NMR first spectral moments for DPPC-d_{62}/egg-PG (7:3) bilayer with (open circle) no protien, (diamond) 16% SP-A and 11% SP-B, and (solid circle) 16% SP-A.

DPPC/egg-PG bilayers. Figure 4.4 shows first spectral moments, M_1, derived from the ^{2}H-NMR spectra shown in figures 4.2 and 4.3, as functions of temperature. In the liquid crystalline phase, far from the transition, the effect of SP-A and SP-B proteins on the acyl chain order is neglegible. SP-A has no effect on the discontinuity of the transition but it does slightly broaden it. In the gel phase of the lipid mixture containing only SP-A, M_1 is slightly lower than for the protein-free lipid mixture. This suggests that SP-A has a slight disordering effect on the phospholipid bilayers. When SP-A and SP-B are present in the bilayer, the first spectral moments in the gel phase increase slightly. It has been previously reported that the values of M_1 for DPPC-d_{62} bilayers in the presence of SP-B are slightly higher than those for the pure

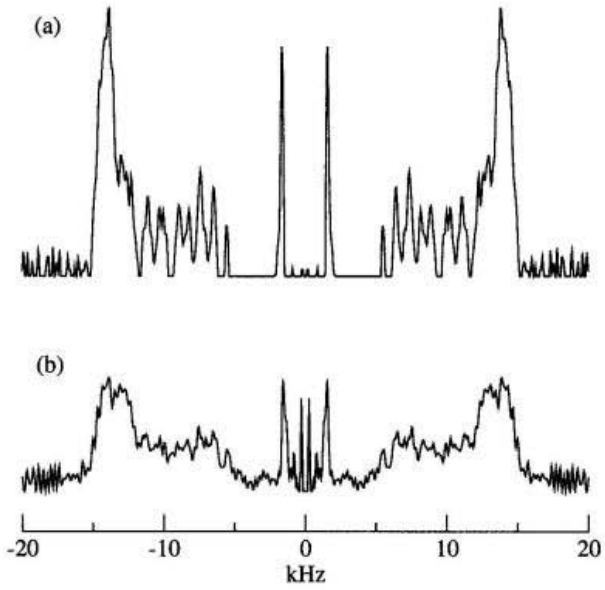

Figure 4.5: DePaked ^{2}H-NMR spectra for DPPC-d_{62}/egg-PG (a) without SP-A and (b) with SP-A.

lipid in the liquid crystalline phase and slightly lower in the gel phase [10]. Again this may suggest that SP-A and SP-B interact in a cooperative manner to remove the effect of PG on DPPC or that the SP-B has has a preferential interaction with PG that reduces its effect on the bilayer order in the gel phase.

The powder pattern spectra can be transformed to yield the spectra that would be seen for an oriented sample using a process known as de-Paking [73]. The de-paking algorithm used produces spectra corresponding to the bilayer normal oriented at 90^o with respect to the magnetic field. Figure 4.5 shows dePaked spectra for DPPC-d_{62}/egg-PG and for the sample containing 16% (w/w) SP-A, both at 45 °C. Near the outer edges of the dePaked spectra there is an overlapping of the quadrupolar splittings corresponding to seven C-^{2}H segments closest to the DPPC glycerol backbone. Further away from the glycerol backbone the acyl chains experience progressively more motional freedom, giving rise to well-resolved peaks. The terminal

methyl groups experience the greatest degree of motional freedom and thus correspond to the smallest quadrupolar splittings. The distribution of resolved doublet splittings is typical of the dependence of orientational order on position along the chain for a range of saturated diacylphosphatidylcholine [74]. There is no qualitative difference in the distribution of deuteron orientational order along the chain. The broadening of the peaks, in the presence of SP-A, likely reflects the reduction in echo decay time.

4.3.2 Deuteron Transverse Relaxation

Additional information about lipid-protein interactions can be obtained from an examination of deuteron transverse relaxation time, T_{2e}, which can indicate how slow molecular reorientation is perturbed by the presence of the protein. Figure 4.7 shows the temperature dependence of T_{2e} for DPPC-d_{62}/egg-PG bilayers and for the sample containing 16% (w/w) SP-A. The transverse relaxation times are obtained by varying the quadrupole echo sequence pulse separation, τ, and taking the initial slope from a semi-logarithmic plot of echo amplitude versus the time at which each echo is formed. Figure 4.6 shows, for example, the quadrupole echo amplitude decays as a function of pulse spacing, 2τ, for DPPC-d_{62}/egg-PG (left) and for the sample with 16 %(w/w) SP-A at selected temperatures. For both samples in figure 4.6, the echo amplitude decay is approximately exponential. Over the temperature range investigated, each of the samples represented in figure 4.7 goes from the liquid crystalline phase, at the highest temperatures, to the gel phase at the lowest temperatures. Figure 4.7 shows that, in the liquid crystalline phase, T_{2e} is approximately constant as the temperature is decreased. As temperature is decreased further, T_{2e} decreases and reaches a minimum at 29 ^{o}C. In the gel phase, as the temperature is decreased, T_{2e} increases

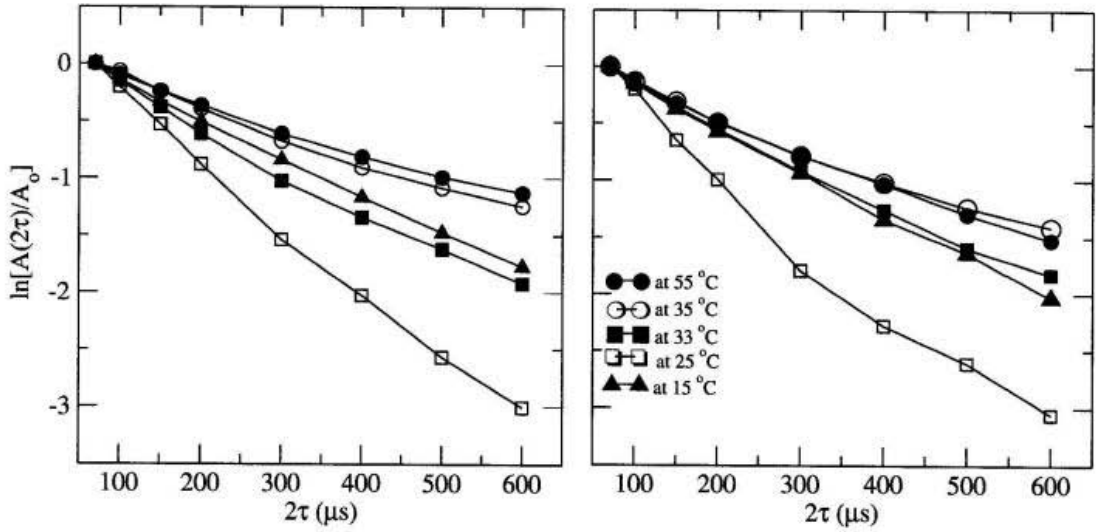

Figure 4.6: Quadrupole echo deacy for DPPC-d_{62}/egg-PG bilayer (*left*) and the sample containing 16% (w/w) SP-A (*right*).

and passes through a maximum. This temperature profile of T_{2e} may, in general, be explained as follows.

Both fast motions (such as chain fluctuation, molecular rotaion, and *trans-gauche* isomerization) and slow motions (such as bilayer surface undulation, lateral diffusion and collective bilayer motion) exist in the liquid crystalline phase. Depending on the order of magnitude of their correlation time, these motions contribute to transverse relaxation rate according to the Equations (2.35) or (2.36) of Chapter 2. The contribution of fast motions to the echo decay rate is proportional to the their correlation time and thus the relaxation rate (time) increases (decreases) with increasing correlation time.

In the liquid crystalline phase, as the sample is cooled and the main phase transition is approached, the increase in correlation times for both fast and slow motions results in opposite effects on echo decay rate as illustrated in figure 4.8. As a result, the contributions from both fast and slow motions tend to cancel the effect of

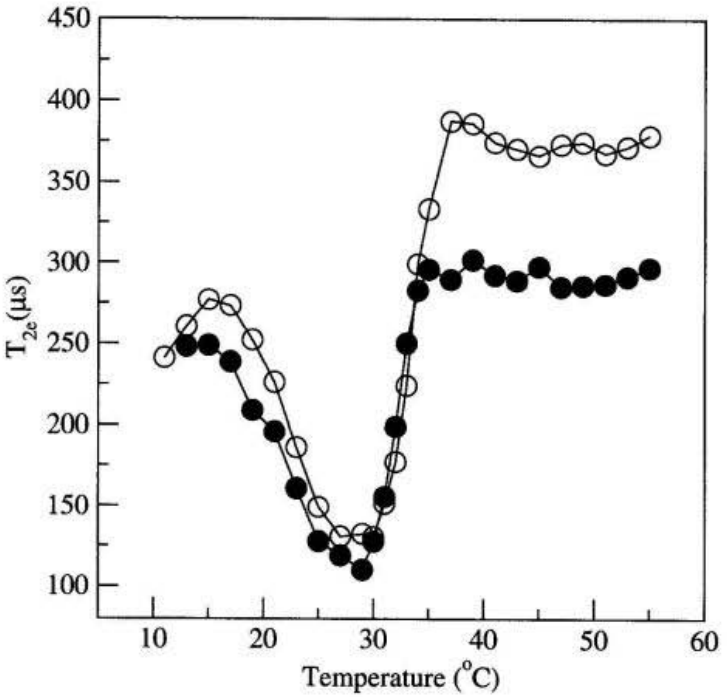

Figure 4.7: Temperature dependence of T_{2e} for DPPC-d_{62}/egg-PG bilayer (open) and the sample containing 16% (w/w) SP-A both hydrated in buffer containing 5 mM Ca^{2+}.

each other such that T_{2e} remains roughly constant with decreasing temperature in the liquid crystalline phase. At the transition or just below it, the correlation time of motions that were fast in liquid crystalline phase become long enough to fall into the slow motions region and their contributions to the transverse relaxation rate become inversely proportional to the correlation time. The relaxation rate then decreases with increasing correlation time so that the echo decay time increases with decreasing temperature. This results in a minimum in average transverse relaxation time near the main transition. Motions which were slow in the liquid crystalline phase, get even slower as the main transition is approached and freeze out in the gel phase. As the correlation times of the motions increase in the gel phase, the transverse re-

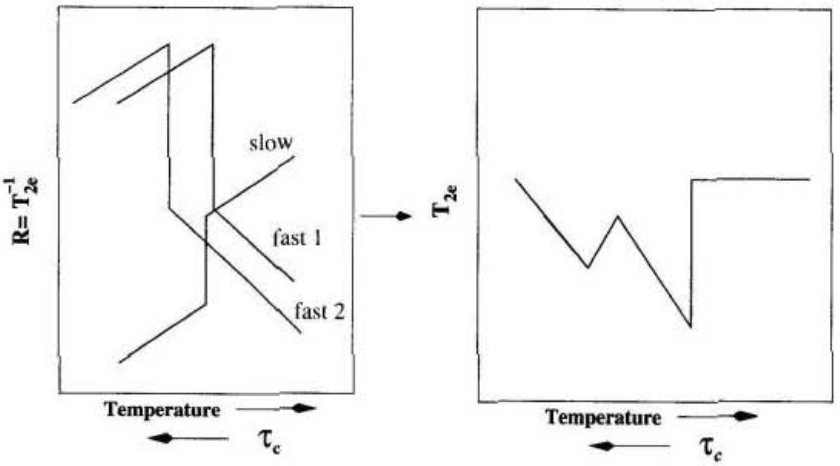

Figure 4.8: Temperature dependence of T_{2e}: Slow and fast motions contribute differently to the relaxation.

laxation rate (time) decreases (increases), reaches a minimum (maximum) and then increases (decreases). This maximum in the gel phase echo decay time suggests the presence of additional fast motions contributing to the relaxation as shown in figure 4.8. Further decrease in temperature leads to an increase in correlation times for the remaining motions in the gel phase and thus the transverse relaxation time decreases.

Figure 4.7 also shows that the addition of SP-A to DPPC-d_{62}/egg-PG bilayers substantially decreases the transverse relaxation time in the liquid crystalline phase but that the effect is much smaller in the gel phase. The decrease in T_{2e} in the liquid crystalline phase indicates that either the correlation times of fast motions become longer or the correlation times of slow motions become shorter due to the presence of SP-A. The former is unlikely because spectral shape or quadrupole splitting remained unchanged in the liquid crystalline phase. As discussed in chapter 2, fast motions cause motional narrowing of the spectrum. If there were significant changes in motional narrowing in the epresence of SP-A, the first spectral moment, which is proportional to the quadrupole splitting, would likely have been affected. Since this

is not observed, as can be seen from figure 4.4 and the dePaked spectra from figure 4.5, SP-A presumably affects mainly slower motions in the liquid crystalline phase.

As mentioned above, SP-A appears to have a very small effect on T_{2e} in the gel phase. This is consistent with the relatively small change in M_1 in the gel phase. In the presence of SP-A, M_1 for DPPC-d_{62}/egg-PG is observed to be lower than for the protein-free mixture. This may be a result of changes in the additional fast motions that appeared in the gel phase. It is interesting to mention here that hydrophobic proteins SP-B and SP-C have much greater effects, in the gel phase, on T_{2e} for phospholipid bilayers [51, 53, 54]

Chapter 5

Results and Discussion II: SP-A Effect on DPPC Headgroup

5.1 Introduction

Chapter 4 discussed the effects of pulmonary surfactant protein SP-A on the hydrocarbon region of DPPC in DPPC/egg-PG bilayers, with and without SP-B, in the presence of Ca^{2+}. The focus of this chapter is on the effect of SP-A on the headgroup region of DPPC in a bilayer consisting of DPPC-d_4/egg-PG in presence of Ca^{2+}. ^{2}H-NMR of headgroup deuterated phosphatidylcholine (PC) has proved to be useful for studying the influence of external perturbations, such as electric charges, hydrostatic pressure, and the addition of surfactant proteins, on the headgroup orientation.

The choline headgroup is approximately parallel to the bilayer surface for pure DPPC bilayers under physiological conditions [56]. The interaction between the phosphatidylcholine $\mathbf{P}^- - \mathbf{N}^+$ dipole and external perturbing surface charge causes the headgroup to tilt toward or away from the bilayer surface depending on the sign of the net surface charge [55, 56, 75, 76]. The headgroup tilts toward or away from the

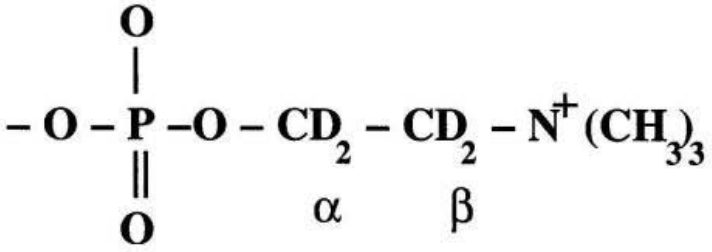

Figure 5.1: The phosphatidylcholine headgroup showing the α and β deuterons. **D** denotes a deuteron.

bilayer surface as its positive quaternary nitrogen is either attracted to or repelled by opposite or like surface charge respectively. This effect, which is termed "molecular voltmeter" has been observed through the quadrupole splittings of deuterons on the α and β carbon of the headgroup. The α and β refer to the choline methylene groups nearest and next nearest, respectively, to the phosphate group as shown in figure 5.1. A headgroup tilt toward the bilayer surface plane causes the α quadrupole splitting to increase and the β quadrupole splitting to decrease, while the tilt away from the bilayer surface plane results in opposite effect on the splittings. The counterdirectional change of the α and β quadrupole splittings is evidence that the response of the headgroup to changes in net surface charge involves in a conformational change rather than ordering or disordering [55, 56, 75, 76]. Tipping of the phosphatidylcholine headgroup in response to external perturbations provides a useful probe of changes in conditions near the bilayer surface.

The effects of the hydrophobic surfactant proteins SP-B and SP-C were previously investigated in our laboratory [12, 78]. It was demonstrated that the interaction of SP-C with the DPPC headgroup is primarily electrostatic in nature. SP-C has three positively charged side chains. The response of headgroup conformation to SP-C concentration was consistent with an interaction between the lipid headgroup dipole

and the net positive charge associated with the protein [12]. Despite the fact that SP-B protein has 9 positively charged and two negatively charged side chains, its interaction with the DPPC headgroup was not expected [78]. Instead of observing an increase in the β quadrupole splittings, addition of SP-B to DPPC leads to a slight decrease in the splittings. It has been suggested that the protein decreases the orientational order slightly which would reduce both α and β quadrupole splittings.

In this chapter, the interaction of SP-A with DPPC deuterated at the α and β positions of the choline headgroup (DPPC-d_4) in DPPC/egg-PG bilayers is discussed.

5.2 Interaction of SP-A with DPPC Headgroup

Figure 5.2 shows ^{2}H-NMR spectra for DPPC-d_4/egg-PG (7:3) with and without 16%(w/w) SP-A, both hydrated in buffer containing 5 mM Ca^{2+}, at selected temperatures. At higher temperatures the spectra are superpositions of Pake doublets which are characterstic of fast axially symmetric reorientation of the headgroup in the liquid crystalline phase. The broader spectrum seen at low temperatures is characteristic of the slower reorientation in the gel phase. The outer and inner doublets arise from pairs of deuterons on the α and β carbons of the choline group, respectively.

The variation of the α and β quadrupole splittings with temperature is presented in figure 5.3. The splittings have been measured between maxima in the dePaked spectra (not shown) corresponding to those shown in figure 5.2. The α quadrupole splittings are unaffected, while the β quadrupole splittings decrease with increasing temperature for both mixtures. In earlier studies of DPPC-d_4 and DMPC-d_4 [77, 78], choline β quadrupole splitting was also observed to decrease with increasing temperature, while the α quadrupole splitting was unaffected. This difference in the response of α and β quadrupole splittings to temperature is due to a combined effect of temperature

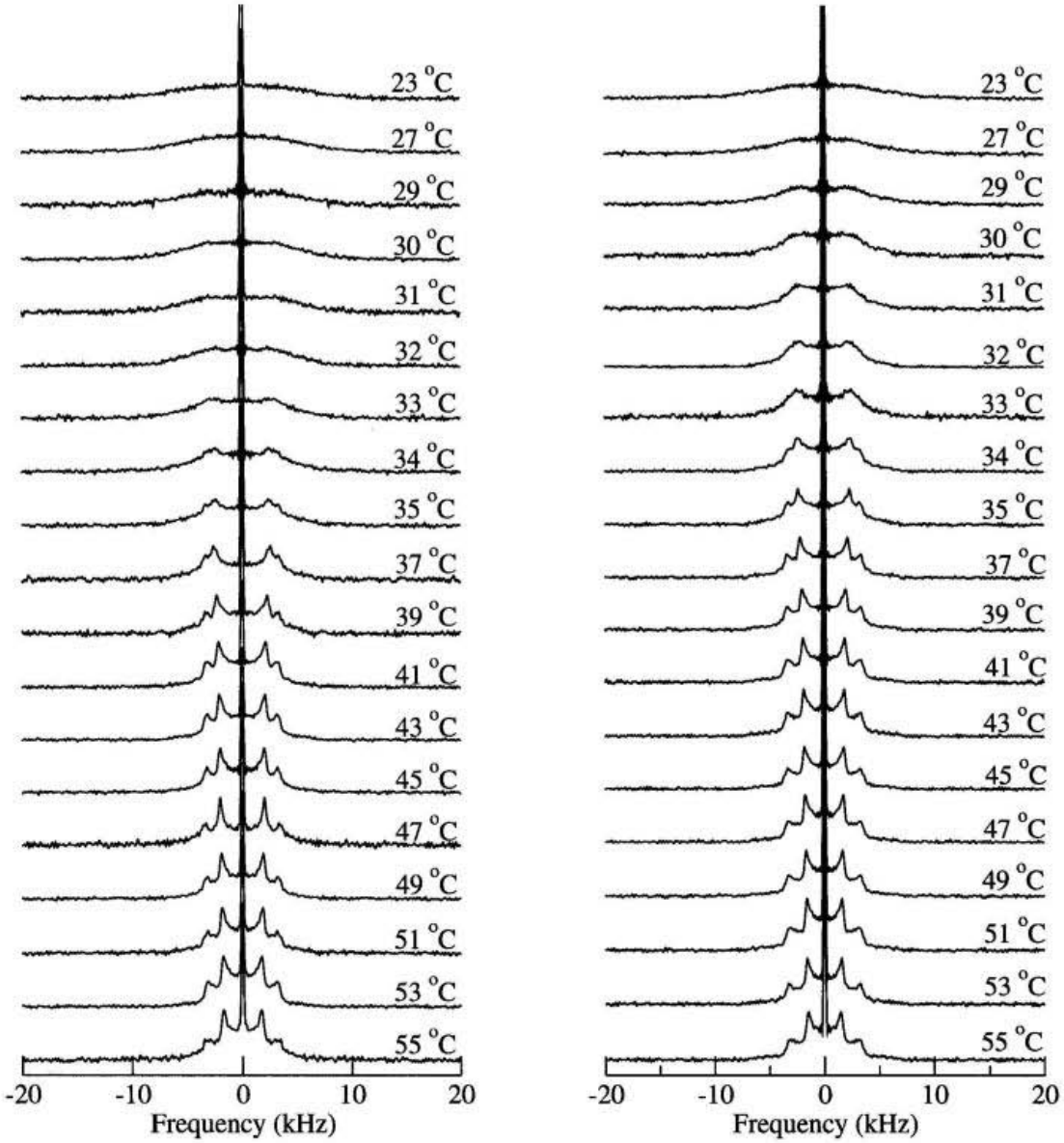

Figure 5.2: Temperature dependence of the ^{2}H-NMR spectrum of DPPC-d_4/egg-PG (7:3) bilayer (*left*) and a bilayer having 16% (w/w) SP–A (*right*) both hydrated in buffer containing 5 mM Ca^{2+} .

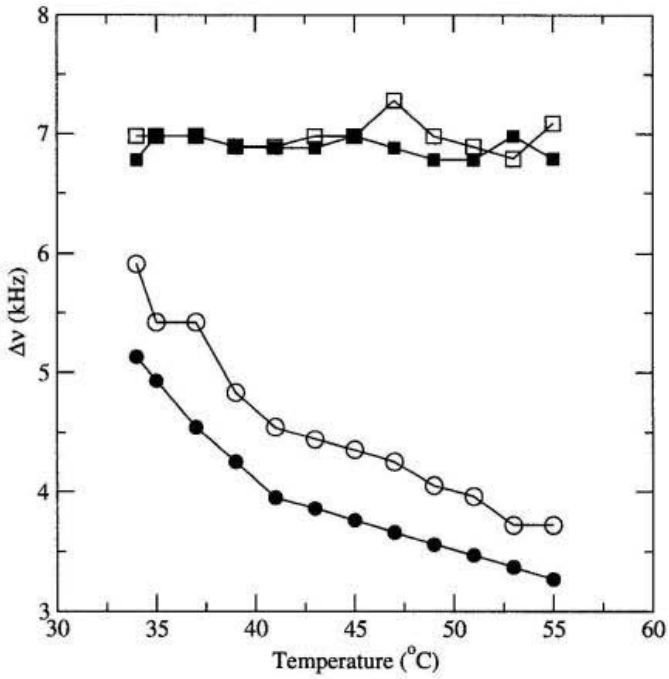

Figure 5.3: Temperature dependence of headgroup deuteron quadrupole splittings for the sample with SP-A (*solid symbols*) and without SP-A (*open symbols*) for the α (*squares*) and β (*circles*) headgroup deuterons.

induced changes in orientational order and area per lipid on headgroup orientation. An increase in temperature may result in an increase in area per lipid and a decrease in orientational order. A tilt of the headgroup toward the bilayer surface due to an increase in area per lipid would increase the α quadrupole splittings and decrease the β quadrupole splittings, while a decrease in orientational order would reduce both splittings. For α deuterons, these two combined effects cancel each other and the observed splittings are unaffected, while these effects are additive for β quadrupole splittings.

Figure 5.3 also shows the effect of SP-A on the DPPC headgroup. It is apparent that SP-A protein reduces the size of the β quadrupole splittings while the α

quadrupole splittings remain unchanged. A decrease in the β quadrupole splittings is indicative of the headgroup tilting toward the bilayer surface. However, another effect occurs at the same time cancelling out the increase in α quadrupole splittings which would expected for this change in orientation.

The application of hydrostatic pressure has been reported to tilt the DMPC headgroup away from the bilayer surface [77]. Application of hydrostatic pressure increases bilayer thickness while reducing area per lipid [77, 79]. On the basis of a comparison with the effect of the hydrostatic pressure on headgroup orientation, it seems that addition of SP-A protein into DPPC-d_4/egg-PG bilayer increases area per lipid. This would be expected to decrease the β quadrupole splittings and increase the α quadrupole splittings. However, the absence of a change in α quadrupole splittings suggests that SP-A also decreases headgroup orientational order. The decrease in orientational order would reduce both splittings. Competition between these two effects could reduce the response of the α quadrupole splittings to the presence of SP-A protein. For β quadrupole splittings, the two effects would be additive.

SP-A induced tilting of the DPPC headgroup, in DPPC-d_4/egg-PG bilayers, toward the bilayer surface is consistent with the effect of SP-A on bilayer packing in the gel phase of DPPC-d_{62}/egg-PG bilayers. The negligible effect of SP-A on bilayer packing in the liquid crystalline phase may not be inconsistent with the small headgroup tilt implied by the decrease in β quadrupole splitting. The highly mobile interface region can apparently accommodate the slight change in headgroup area, perhaps by displacing water, without affecting chain packing. In the gel phase, the area available for the headgroup is smaller and accommodation of the increased area seems to interfere with chain packing. The results described here and in the previous chapter may suggest that SP-A primarily interacts with the DPPC/egg-PG bilayer surface.

Chapter 6

Summary and Concluding Remarks

Interaction of the hydrophilic protein A (SP-A) with the DPPC/egg-PG bilayer was studied by using ^{2}H-NMR spectroscopy in two ways. First we looked at how SP-A, with or without SP-B, in the presence of Ca^{2+} affects the orientational order, phase behaviour, and dynamics of the acyl chains of DPPC in a bilayer comprised of DPPC/egg-PG (7:3). Secondly, we looked at how this protein interacts with the DPPC headgroup in the bilayers.

When incorporated into DPPC-d_{62}/egg-PG bilayers, SP-A was found to have no effect on the bilayer's phase transition. DPPC-d_{62}/egg-PG bilayers with or without SP-A were found to exhibit a continuous liquid crystal-to-gel phase change. Pure DPPC-d_{62} bilayers display a sharp transition form liquid crystal-to-gel phase at 37^{o}C. Addition of egg-PG to DPPC resulted in the transition proceeding continuously. This indicates that SP-A does not have a preferential interaction with one or the other lipid components of the DPPC-d_{62}/egg-PG bilayers. However, SP-A was found to interfere with lipid packing in the gel phase. This was reflected by lower values of M_1, in the

gel phase, compared to those for the protein-free bilayer.

When SP-A was present together with the hydrophobic protein SP-B in DPPC-d_{62}/egg-PG bilayers, a relatively sharp transition was observed. Taken together with the observations mentioned above, this suggests that both proteins interact in a co-operative manner such that the effect of egg-PG is removed. Previous results from our laboratory showed that the presence of SP-B in DPPC-d_{62} bilayer results in the transition proceeding continuously. Thus, another possibility is that SP-B has a preferential interaction with the egg-PG that reduces its effect on the bilayer. M_1 values for DPPC-d_{62}/egg-PG (7:3)/16 %(w/w) SP-A /10 %(w/w) SP-B were observed to be slightly higher than those for the protein-free mixture which indicated that the bilayer became more ordered than protein-free bilayers. Again this suggests that SP-A and SP-B work together to pack the DPPC-d_{62}/egg-PG bilayers.

The temperature dependence of T_{2e} illustrated that the presence of SP-A in the bilayer had an effect on bilayer slow motions in the liquid crystalline phase. This was revealed by the observation that T_{2e} for DPPC-d_{62}/egg-PG/SP-A is much lower than for the mixture without SP-A. Surprisingly, SP-A was found to have little effect on echo decay in the gel phase.

The effect of SP-A on DPPC headgroup orientation was studied by collecting ^{2}H-NMR spectrum for DPPC-d_4/egg-PG (7:3) with and without SP-A at selected temperatures. From their dePaked spectra, we then measured the DPPC headgroup choline α and β deuteron quadrupole splittings. The presence of SP-A protein resulted in a reduction of the β deuteron quadrupole splittings and the α quadrupole splittings remained unchanged. This was taken as an indication of the presence of counter acting effects which tend to influence the α and β quadrupole splittings in such a way that the changes in α quadrupole splittings were cancelled out and those in β quadrupole splittings were reinforced. This was found to be consistent with the increase in area

per lipid and the decrease in the headgroup orientational order.

The effect of SP-A on DPPC-d_4/egg-PG bilayer, implied by the headgroup deuterons' quadrupole splittings, is consistent with that reported on DPPC-d_{62}/egg-PG bilayer acyl chains. The temperature dependence of the first spectral moment (M_1) indicated that SP-A protein has a disordering effect on the bilayer in the gel phase. Headgroup observations also indicated that SP-A has that effect but this time in the liquid crystalline phase.

In comparison with previous ^{2}H-NMR studies of phospholipid-protein interaction [10, 12, 31, 51, 53, 54], the hydrophilic protein SP-A, and the hydrophobic proteins SP-B and SP-C had similar effects in the liquid crystalline phase. Each protein had no noticeable effect on phospholipid acyl chain orientational order and they were reported to lower the transverse relaxation time on the liquid crystalline phase [10, 51, 53, 54]. They have some differences in effects in the gel phase. While SP-B, in the absence of Ca^{+2}, was found to lower the transverse relaxation time for DPPC/DPPG-$_{62}$ (70:30) and have no effect on the chain order in the gel phase [54, 78], SP-C was found to affect both the echo decay and the chain order of DPPC/DPPG-$_6$2 (70:30) [53, 78]. Results presented in this thesis illustrate that SP-A had a disordering effect on the phospholipid bilayers in the gel phase but its effect on the echo decay is negeligible in comparison with its effect in the liquid crystalline phase.

Bibliography

[1] L. A. Creuwels, L. M. van Golde, and H. P. Haagsman, *Lung* **175**, 1-39 (1997).

[2] J. A. Clements, *Am. Rev. Respir. Dis.* **115**, 67-71 (1977).

[3] K. M. W. Keough, *in Pulmonary Surfactant: from Molecular Biology to Clinical Practice, Elsevier Science Publishers*, 109-163 (1992).

[4] T. Akino, *in Pulmonary Surfactant: from Molecular Biology to Clinical Practice, Elsevier Science Publishers*, 19-31 (1992).

[5] J. A. Whitset and T. E Waver, *in Pulmonary Surfactant: Biochemical, Fumctional, Requlatory and Clinical Concepts, CRC Press, Inc*, 77-104 (1991).

[6] T. E. Weaver, and J.A Whitsett, *Biochem. J.* **273**, 249-264 (1991).

[7] E. C. Crouch, *Respir. Res.* **1**, 93-108 (2000).

[8] J. Johansson, T. Curstedt, and B. Robertson, *Eur. Respir. J.* **7**, 364-372 (1994).

[9] T. Curstedt, J. Johansson, J. Barros - Söderling, B. Robertson, G. Nilsson, M. Westberg, and H. Jörnval, *Eur. J. Biochem.* **172**, 521-525 (1988).

[10] M. R. Morrow, J. Pérez-Gil, G. Simatos, C. Bonland, J. Stewart, D. Absolom, V. Sarin, and K. M. W. Keough, *Biochemistry* **32**, 4397-4402 (1993).

[11] J. Johansson, T. Szyperski, T. Cursted, K. Wüthrich, *Biochemistry* **33**, 6015-6023 (1994).

[12] M. R. Morrow, S. Taneva, G. A. Simatos, L. A. Allwood, and K. M. W. Keough, *Biochemistry* **32**, 11338-11344 (1993).

[13] B. Pastranat, A. J. Mautone, and R. Mendelson, *Biochemistry* **30**, 10058-10064 (1991).

[14] G. Vandenbussche, A. Clercx, T. Curstedt and J. Johansson, H. Jörnval, and J. M Ruysschaert, *Eur. J. Biochem.* **203**, 201-209 (1992).

[15] S. Hawgood, *in Pulmonary Surfactant: from Molecular Biology to Clinical Practice, Elsevier Science Publishers*, 33-54 (1992).

[16] R. J. King, and J. A. Clements, *Am. Rev. Respir. Dis.* **115**, 67-71 (1977).

[17] R. T. White, D. Damm, J. Miller, K. Spratt, J. Schilling, S. Hawgood, B. Bemson, and B. Cordell, *Nature (London)* **317** 361-363 (1985).

[18] K. R. Khubchandani, and J. M. Snyder, *FASEB J.* **15**, 59-69 (2001).

[19] J. Floros, R. Steinbrink, K. Jacobs, D. Phelps, R. Kriz, M. Recncy, L. Sultzman, S. Jones, H. W. Taeuch, H. A. Frank, and E. F. Fristch, *J. Biol. chem.* **261**, 9029-2033(1986).

[20] T. Voss, K. Melchers, G. Scheirle, and K. P. Schafer, *J. Respir. Cell Mol. Biol.* **4** 88-94 (1991).

[21] H. P. Haagsman, S. Hawgood, T. Sargean, D. Buckley, R. T. White, K. Drickamer, and B. J. Benson, *J. Biol. Chem.* **262** 13877-13880 (1987).

[22] N. Palaniyer, R. A. Risdale, C. E. Holterman, K. Inchley, F. Possmayer, and G. Harauz, *Am. J. Structural Biol.* **122**, 297-310 (1998).

[23] N. Palaniyer, F. X. McCormack, F. Possmayer, and G. Harauz, *Biochemistry* **39**, 6310-6316 (2000).

[24] J. M. Snyder, J. M. Johanson, and C. R. Mendelson, *Cell Tissu Res.* **220**, 17-24 (1981).

[25] J. R. Bourbon, *in Pulmonary Surfactant: Biochemical, Fumctional, Requlatory and Clinical Concepts, CRC Press, Inc*, 143-183 (1991).

[26] N. Palaniyer, R. A. Risdale, S. A. Hearn, F. Possmayer, and G. Harauz, *Am. J. Physiol.(Lung Cell. Mol. Physiol. 20)* **276**, L642-L649 (1999).

[27] J. R. Bourbon, *in Pulmonary Surfactant: Biochemical, Fumctional, Requlatory and Clinical Concepts, CRC Press, Inc*, 37-76 (1991).

[28] N. Palaniyer, R. A. Risdale, S. A. Hearn, Y. M. Heng, *Am. J. Physiol.(Lung Cell. Mol. Physiol. 20)* **276**, L631-L641 (1999).

[29] Y. Suzuki, Y. Fujita, and K. Kogishi, *Am. Rev. Respir. Dis.* **140**, 75-81 (1989).

[30] M. C. Williams, S. Hawgood, and R. L. Hamilton *Am. J. Respir. Cell Mol. Biol.* **5**, 41-50 (1991).

[31] M. R. Morrow, S. Harris, J. Stewart, S. Taneva, A. Dico, N. Abu-Libdeh, J. Walter, and K. M. W. Keough, *submitted to Biophysical Journal.*

[32] L-A. D. Worthman, K. Nag, N. Rich, M. L. F. Ruano, C. Casals, J. Pérez-Gil, and K. M. W. Keough, *Biophys. J.* **79**, 2657-2666 (2000).

[33] S-H. Yu, F. X. McCormack, D. R. Voelker, and F. Possmayer, *J. Lipid Res.* **40**, 920-929 (1999).

[34] S-H. Yu, and F. Possmayer, *J. Lipid Res.* **39**, 555-568 (1998).

[35] C. Casals, E. Miguel, and J. Pérez-Gil, *Biochem. J.* **296**, 583-593 (1993).

[36] J. E. Baatz, V. Sarin, D. R. Absolom, C. Baxter, and J. A. Whitsett. *Chem. Phys. Lipids.* **60**, 163-178 (1991).

[37] A. D. Horowitz, B. Elledge, J. A. Whitsett, and J. E. Baatz *Biochim. Biophys. Acta* **1107**, 44-54 (1992).

[38] H. P. Haagsman, R. V. Diemel, *Comp. Biochem. Phys.*(Molecular and Integrative Physiology) **276**, 91-108 (2001).

[39] T. Curstedt, H. Jörnval, B. Robertson, T. Bergman, and P. Berggren, *Eur. J. Biochim.* **168**, 255-262 (1987).

[40] S-H. Yu, and F. Possmayer, *Biochem. Biophys. Acta* **1046**, 233-241 (1990).

[41] W. F. Voorhout, T. Veenendaal, H. P. Haagsman, A. J. Verkleij, L. G. M. van Gold, and H. J. Geuze, *J. Histochem Cytochem* **39**, 1331-1336 (1991).

[42] S. Hawgood, B. J. Benson, J. Schilling, D. Damm, J. A. Clements, and R. T. White, *Proc. Natl. Sci. Aca. U.S.A.* **84** 66-70 (1987).

[43] Y. Kurko, and T. Akino, *J. Biol. Chem.* **266**, 3068-3073 (1991).

[44] J. R. Wright, R. E. Wager, S. Hawgood, L. Dobbs, and J. A. Clements, *J. Biol. chem* **262**, 2888-2894 (1987).

[45] M. A. Oosterlaken-Dijkserhuis, H. P. Haagsman, L. M. G. van Gold, and R. A. Damel. *Biochemistry* **30**,10965-10971(1991).

[46] J. Pérez-Gil, C. Casals, and D. Marsha, *in NATO ASI Series, H82, Biological Membranes: Structure, Biogenesis and Dynamics*, (edit by J. A. F. Kamp), Springer - Verlag, Berlin, 93-100 (1994).

[47] J. S. Vincent, S. D. Revak, C. G. Cochrane, and I. W. Levin. *Biochemistry* **30**, 8395-8401 (1991).

[48] J. S. Vincent, S. D. Revak, C. G. Cochrane, and I. W. Levin. *Biochemistry* **32**, 8228-8238 (1993).

[49] S. L. Krill, S. L. Gupta, and T. Smith. *Chem. Phys. Lipids.* **71**, 47- 49 (1991).

[50] K. Shiffer, S. Hawgood, H. P. Haagsman, B. Benson, J. A. Clements, and J. Goerke. *Biochemistry* **32**, 590-597 (1993).

[51] G. Simatos, K. B. Forward, M. R. Morrow, and K. M. W. Keough, *Biochemistry* **29**, 5807-5814 (1990).

[52] J. Pérez-Gil, C. Casals, and D. Marsha, *Biochemistry* **34**, 3964-3971 (1995).

[53] A. S. Dico, S. Taneva, M. R. Morrow, and K. M. W. Keough, *Biophys. J.***73**, 2595-2602 (1997).

[54] A. S. Dico, J. Hankock, M. R. Morrow, J. Stewart, S. Harris, and K. M. W. Keough, *Biochemistry* **36**, 4172-4177 (1997).

[55] P. G. Scherer, and J. Seelig, *Biochemistry* **28**, 7720-7728 (1989).

[56] J. Seelig, P. M. Macdonald, and P. G. Scherer, *Biochemistry* **26**, 7535-7541 (1987).

[57] *Hand Book Of Chemistry and Physics*, 51st edition, edited by R. C. Weast. The Chemical Rubber Co., Ohio (1970).

[58] J. H. Davis, *Biochimica et Biophysica Acta* **737**, 117-171 (1983).

[59] M. Bloom, and E. Evans, *in Biologically Inspired Physics,* edited by L. Peliti, Plenum Press, New York, 137-146 (1992).

[60] J. H. Davis, *Chem. Phys. Lipids* **40**, 223-258 (1983).

[61] J. H. Davis, *Isotopes in Physicsal and Biomedical Science*, Volume 2. Elsevier Science Publishers, Amsterdam (1991).

[62] C. P. Slichter, *Principle of Magnetic Resonance*, edited by P. Fulde, Springer Verlag, Springer Series in Solid State Science 1 (1983).

[63] J. Seelig, *Quarterly Reviews of Biophysics.* **10**, 353-418 (1977).

[64] J. H. Davis, K. R. Jeffrey, M. Bloom, M. I. Valic, and T. P. Higgs, *Chem. Phys. Let.* **42**, 390-394 (1976).

[65] M. Bloom, C. Morrison, E. Sternin, and J. L. Thewalt, *In pulsed Magnetic Resonance: NMR, ESR, and Optics,* edited by D. M. S. Bagguley, Clarendon Press, Oxford, 274-316 (1992).

[66] J. R. Y. Dong, *Nuclear Magnetic Resonance of Liguid Crystals*, Spring-Verlag (1994).

[67] K. P. Pauls, A. L. Mackay, O. Söderman, M. Bloom, A. K. Tanjea, and R. S. Hodges. *Eur. Biophys. J.* **12**, 1-11(1985).

[68] M. Bloom and E. Sternin, *Biochemistry* **26**, 2101-2105 (1987).

[69] J. Stohrer, G. Grobner, D. Reimer, K. Weisz, C. Mayer and G. Kothe, *J. Chem. Phys.* **95**, 672-678 (1991).

[70] P. Meier, E. Ohmes and and G. Kothe *J. Chem. Phys.* **85**, 3598-3614(1986).

[71] D. I. Hoult, *Progress in NMR Spectroscopy* **12**, 44-77 (1978).

[72] R. S. Prosser, J. H. Davis, F. W. Dahlquist and M. A. Lindorfer, *Bichemistry* **30**, 4687-4696 (1991).

[73] E. Sternin, M. Bloom, A. L. MacKay, *J. Magn. Res.* **55**, 274-282 (1993).

[74] M. R. Morrow, and D. Lu, *Chem. Phys. Lett.* **182**, 435-439 (1991).

[75] P. M. Macdonald, J. Leisen, and F. M. Marassi, *Biochemistry* **30**, 3558-3566 (1991).

[76] P. M. Macdonald, and J. Seelig, *Biochemistry* **26**, 1231-1240 (1987).

[77] B. B. Bonev, and M. R. Morrow, *Biophys. J.* **69**, 518-523 (1995).

[78] A.S. Dico, *Ph.D Thesis*, Memorial University of Newfoundland, St. John's (1997).

[79] L. F. Braganza, and D. L. Worcester, *Biochemistry* **25**, 2591-2595 (1986).